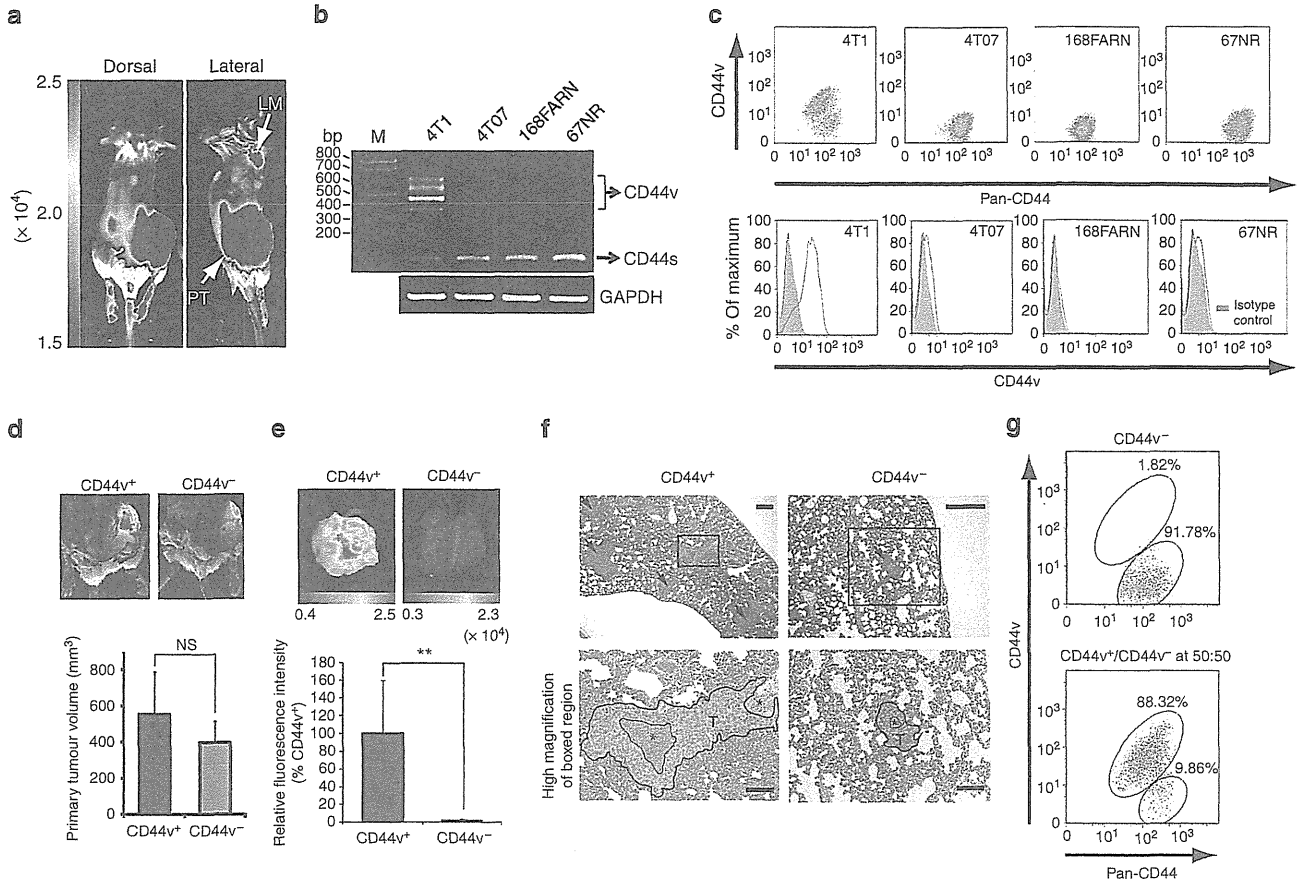

Figure 1 | Expression of CD44v in metastatic breast cancer cells with lung colonization potential. (**a**) IntegriSense fluorescence images of a representative mouse injected with 4T1 cells (1×10^5) orthotopically into the mammary gland. Left colour bar and associated numbers indicate fluorescence intensity levels, with red and blue representing high and low fluorescence signals, respectively. LM, lung metastasis; PT, primary tumour. (**b**) RT-PCR analysis of total RNA from the indicated cell lines with primers targeted to exons 5 and 16 of the mouse *CD44* gene as well as to the mouse *glyceraldehyde-3-phosphate dehydrogenase* (*Gapdh*) gene (internal control). M, DNA size marker. (**c**) Flow cytometric analysis of CD44 isoform expression on the indicated cell lines with antibodies that recognize all isoforms of CD44 (pan-CD44) or only CD44v. Similar results were obtained in three independent experiments. (**d**) IntegriSense images of primary tumours formed as a result of orthotopic injection of sorted $CD44v^+$ or $CD44v^-$ 4T1 cells (1×10^5) into the mammary gland of mice (upper). Tumour volume at 30 days after cell injection was calculated as length×$(width)^2/2$ (bottom), and data are means ±s.d. for eight animals per group. NS, not significant. (**e**) IntegriSense images of lung metastases formed in mice injected as in (**d**), and quantitative analysis of the total fluorescence intensity per lung metastatic lesion. Quantitative data are means±s.d. for 5 animals injected with $CD44v^+$ cells or $CD44v^-$ cells. $^{**}P<0.01$ (Student's *t*-test). (**f**) Haematoxylin-eosin staining of lung metastases formed 30 days after orthotopic injection of $CD44v^+$ or $CD44v^-$ cells into the mammary gland of recipient mice. The boxed regions in the upper panels are shown at higher magnification in the lower panels. Arrows indicate metastatic nodules in the lung; asterisks indicate blood vessels; T, tumour. Scale bars, 300 μm (upper) or 100 μm (lower). (**g**) Flow cytometric analysis of CD44 isoform expression on tumour cells (6-TG-resistant and lineage marker-negative (Lin^-) cells) isolated from lung metastases at 30 days after intravenous injection of $CD44v^-$ 4T1 cells (1×10^4) or both $CD44v^+$ and $CD44v^-$ 4T1 cells (5×10^3 cells each).

15/15; shESRP1 $CD44v^+$, 15/15) and volume (Fig. 2f) of primary tumours formed by these cells were similar, the incidence of lung metastasis was reduced for the ESRP1-depleted cells (shC $CD44v^+$, 14/15; shESRP1 $CD44v^+$, 6/15). Furthermore, the extent of lung metastases was reduced for shESRP1 $CD44v^+$ cells compared with shC $CD44v^+$ cells (Fig. 2g), suggesting that ESRP1 promotes lung colonization by $CD44v^+$ 4T1 cells.

$CD44v^+$ stem-like cells dominantly colonize and expand in the lung. We next examined whether metastasis-associated stress results in enrichment of ROS-resistant cells. We isolated tumour cells from the primary lesion (4T1PT) and lung metastases (4T1LM) formed by 4T1 cells (Fig. 3a) and evaluated their intracellular ROS levels by staining with the fluorescent probe 2′,7′-dichlorofluorescein diacetate (DCFH-DA). ROS levels of 4T1LM cells were lower than those of 4T1PT cells in the absence or presence of hydrogen peroxide (H_2O_2) (Fig. 3b; Supplementary Fig. S2), indicating that 4T1LM cells have a higher ROS-defence capacity than 4T1PT cells. Furthermore, flow cytometry of cells labelled with 5-chloromethylfluorescein diacetate (CFMDA), a fluorescent probe for GSH (Supplementary Methods), revealed that intracellular GSH abundance in 4T1LM cells was greater than that of 4T1 or 4T1PT cells (Fig. 3c). A luminescence-based assay that relies on the conversion of a luciferin derivative to luciferin in the presence of GSH[18] also showed that the intracellular GSH content of 4T1LM cells was significantly greater than that of 4T1PT cells (Supplementary Fig. S2). Together, these results indicated that lung metastasis results in enrichment of ROS-resistant cells with high GSH levels. To examine whether CD44v-expressing cells maintain high GSH levels *in vivo*, we applied imaging mass spectrometry to visualize GSH and oxidized glutathione (GSSG) in frozen tissue samples[34,35]. $CD44v^+$ lung metastases formed by 4T1 cells manifested high levels of GSH but not of GSSG (Fig. 3d),

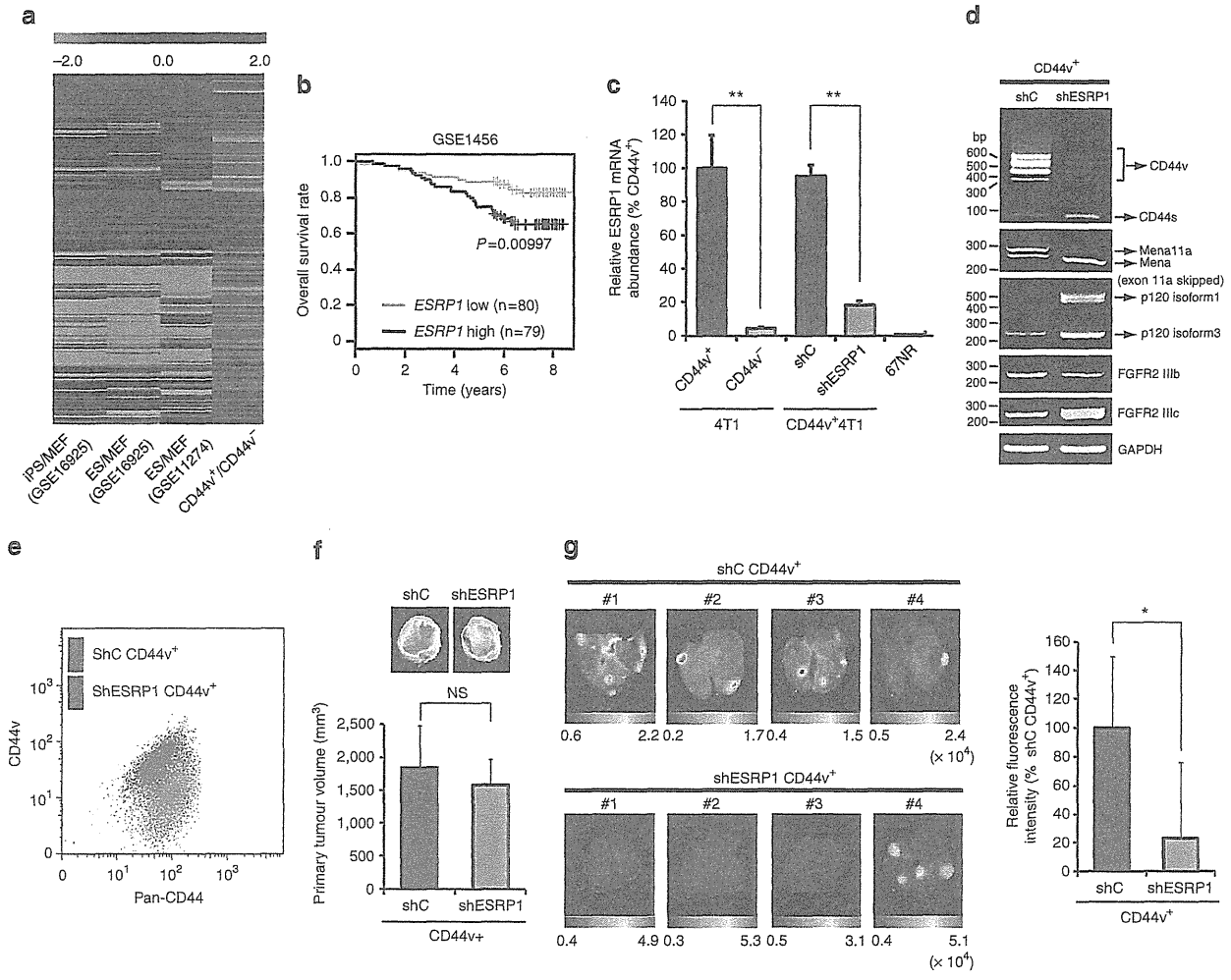

Figure 2 | Regulation of alternative splicing of CD44 mRNA and promotion of lung metastasis by ESRP1. (**a**) GSEA of microarray data for CD44v$^+$ cell/CD44v$^-$ cell, ES cell/MEF (GSE16925 and GSE11274), and iPS cell/MEF (GSE16925) profiles. (**b**) Kaplan–Meier plots of overall survival according to *ESRP1* (219121_s_at) expression level for a breast cancer patient set (GSE1456, $n=159$). (**c**) Quantitative RT-PCR analysis of the abundance of *ESRP1* mRNA in CD44v$^-$ 4T1 cells, shC CD44v$^+$ cells, shESRP1 CD44v$^+$ cells, and 67NR cells relative to that in CD44v$^+$ 4T1 cells. Data were normalized by the amount of *Gapdh* mRNA and are means±s.d. from three independent experiments. $^{**}P<0.01$ (Student's *t*-test). (**d**) RT-PCR analysis of splice variant mRNAs for *CD44*, *Mena*, *p120 catenin*, and *FGFR2* in shC CD44v$^+$ and shESRP1 CD44v$^+$ cells. (**e**) Flow cytometric analysis of CD44 expression on shC CD44v$^+$ and shESRP1 CD44v$^+$ cells with antibodies to pan-CD44 and to CD44v. (**f**) IntegriSense images of primary tumours formed in mice by orthotopically injected shC CD44v$^+$ or shESRP1 CD44v$^+$ cells (1×10^5) as well as tumour volume at 30 days after cell injection. Quantitative data are means±s.d. for five animals per group. (**g**) IntegriSense images of lung metastases and quantitative analysis of the total fluorescence signal intensity per lung metastatic lesion for mice injected as in (**f**). Quantitative data are means±s.d. for four animals per group. $^*P<0.05$ (Student's *t*-test).

suggesting that CD44v confers ROS resistance to cancer cells through the promotion of GSH synthesis. We then examined the role of GSH in lung colonization by CD44v$^+$ cells with the use of L-buthionine sulphoximine (BSO), which inhibits γ-glutamylcysteine synthase[36] and thereby depletes intracellular GSH (Supplementary Fig. S2). Lung colonization by L-buthionine sulphoximine-treated CD44v$^+$ cells was significantly inhibited compared with that of control cells (Supplementary Fig. S2), suggesting that a high intracellular GSH level enhances the lung colonization potential of CD44v$^+$ cells.

Breast cancer stem cells manifest an increased ROS defence capacity relative to their nontumorigenic progeny[37]. We therefore examined 4T1LM cells for the presence of stem-like cells with the use of ALDEFLUOR, a fluorescent probe for aldehyde dehydrogenase (ALDH) activity, a marker for stem-like cancer cells[38]. 4T1LM cells contained a much larger proportion of ALDEFLUOR-positive cells compared with 4T1 or 4T1PT cells (Fig. 3e). Furthermore, most ALDEFLUOR-positive 4T1LM cells expressed CD44v (Fig. 3f), suggesting that CD44v$^+$ stem-like cells may expand during lung colonization. In contrast, the proportions of ALDEFLUOR-positive cells among noninjected CD44v$^+$ or CD44v$^-$ 4T1 cells were similar (Fig. 3g). These results suggested that the difference in metastatic behaviour between CD44v$^+$ and CD44v$^-$ cells is determined by the difference in ROS resistance rather than by a difference in the size of the pre-existing stem-like cell population.

CD44 splicing enhances ROS defence in metastatic 4T1 cells. We examined the role of xCT in lung metastasis and found that the level of xCT expression on the surface of 4T1 cells was greater than that on 67NR (nonmetastatic) cells (Fig. 4a). It was also higher on CD44v$^+$ cells compared with CD44v$^-$ cells. xCT was downregulated on CD44v$^+$ cells by RNA interference-mediated depletion of ESRP1 (Fig. 4b), suggesting that ESRP1-dependent splicing of CD44 mRNA controls the cell surface expression of xCT. Consistent with these results (Fig. 4a,b), the intracellular GSH content was

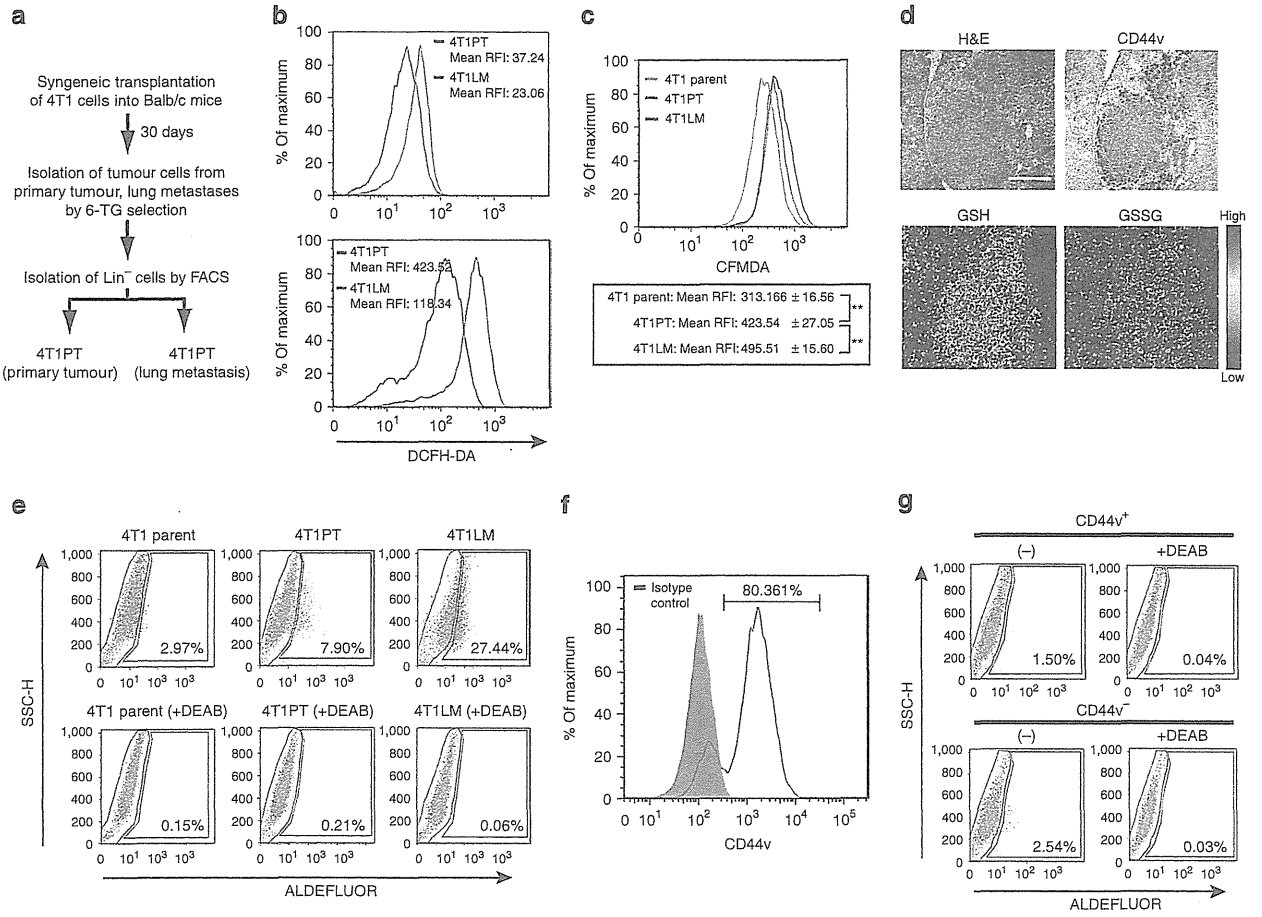

Figure 3 | Selective expansion of CD44v⁺ stem-like cancer cells during lung metastasis. (**a**) Experimental protocol. (**b**) 4T1PT or 4T1LM cells were incubated with or without 500 μM H_2O_2 for 20 min, stained with DCFH-DA, and subjected to flow cytometric analysis. RFI, relative fluorescence intensity. Similar results were obtained in three independent experiments. (**c**) Flow cytometric analysis of parental 4T1 as well as 4T1PT and 4T1LM cells stained with CFMDA (upper). Mean±s.d. values for RFI from five independent experiments are also shown (lower); $^{**}P<0.01$(Student's *t*-test). (**d**) Haematoxylin-eosin (H&E) staining and immunohistochemical staining of CD44v (upper panels) as well as imaging mass spectrometry of GSH and GSSG (lower panels) in lung metastases formed by 4T1 cells. The colour bar indicates peak intensity levels at *m/z* 306.0 (GSH) or 611.1 (GSSG), with red and blue representing high and low signals, respectively. Scale bar, 500 μm. (**e**) Flow cytometry of 4T1, 4T1PT, or 4T1LM cells incubated with the ALDEFLUOR substrate (BAAA) with or without the specific inhibitor (DEAB) to establish the baseline fluorescence and to define the ALDEFLUOR-positive region. SSC-H, side scatter. (**f**) Flow cytometric analysis of CD44v expression in ALDEFLUOR-positive 4T1LM cells. Cells were stained with antibodies to CD44v after incubation with BAAA in the absence or presence of DEAB. Similar results were obtained in three independent experiments. (**g**) Flow cytometric analysis of CD44v⁺ or CD44v⁻ 4T1 cells subjected to the ALDEFLUOR assay as in (**e**). Similar results were obtained in three independent experiments.

significantly higher for 4T1 cells than for 67NR cells, for CD44v⁺ cells compared with CD44v⁻ cells, and in shC CD44v⁺ cells compared with shESRP1 CD44v⁺ cells (Fig. 4c). These findings suggested that ESRP1-regulated CD44v expression increases the amount of xCT at the cell surface and thereby contributes to the maintenance of high GSH levels. To investigate whether xCT activity promotes lung colonization by CD44v-expressing cells, we examined the effect of the specific xCT inhibitor sulfasalazine (Supplementary Methods)[18,39]. Two weeks after intravenous injection of CD44v⁺ cells, lung metastasis was suppressed in sulfasalazine-treated mice compared with saline-treated controls (Fig. 4d), suggesting that xCT has a functional role in lung colonization.

ESRP1 affects the splicing of mRNAs for various proteins including FGFR2, p120 catenin, and Mena as well as CD44 (ref. 14). To examine the contribution of CD44v to ESRP1-dependent lung metastasis, we introduced CD44v8-10 complementary DNA[18] into shESRP1 CD44v⁺ cells to generate cells that stably express CD44v8-10 as well as ESRP1 shRNA (Fig. 4e; Supplementary Fig. S3). Cells expressing CD44v8-10 showed a significantly higher level of GSH compared with cells transfected with the empty vector (Fig. 4f). Furthermore, the increase in ROS level after exposure to H_2O_2 was reduced by forced expression of CD44v8-10 (Fig. 4g), indicating that CD44v8-10 expression enhanced ROS defence in ESRP1-depleted cells. ROS abundance in the absence of H_2O_2 was not affected by CD44v8-10 expression (Supplementary Fig. S3), suggesting that CD44v8-10 protects cancer cells on exposure to excessive amounts of ROS.

Finally, forced expression of CD44v8-10 resulted in a marked increase in the lung metastatic potential of ESRP1-depleted cells (Fig. 4h). Together, these data suggested that alternative splicing of CD44 mRNA regulated by ESRP1 enhances xCT-dependent ROS defence in cancer cells and thereby promotes efficient lung colonization.

Epigenetic regulation of *ESRP1* expression in 4T1 cells. ESRP1 expression was recently shown to be downregulated in cells

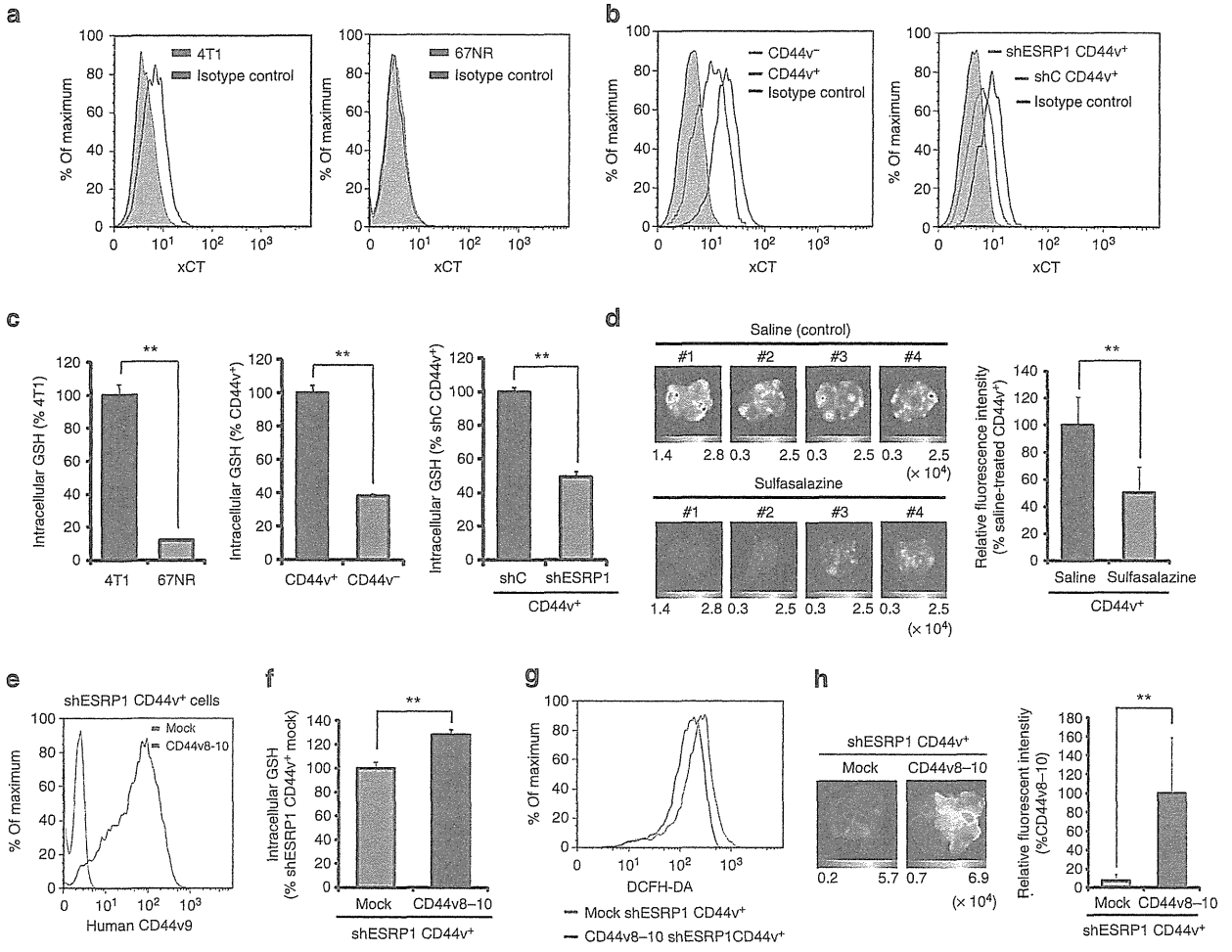

Figure 4 | CD44 splicing enhances ROS defence and lung colonization potential. (**a**) Flow cytometric analysis of xCT expression on 4T1 or 67NR cells. (**b**) Flow cytometry of xCT expression on CD44v$^+$ or CD44v$^-$ 4T1 cells (upper left) and on shC CD44v$^+$ or shESRP1 CD44v$^+$ cells (upper right). CD44v$^-$ (Mean RFI; 6.72±0.14), CD44v$^+$ (Mean RFI; 10.06±0.93**). shESRP1 CD44v$^+$ (Mean RFI; 6.09±0.29), shC CD44v$^+$ (Mean RFI; 9.41±0.44**). Mean ±s.d. values for RFI from five independent experiments. **$P<0.01$ (Student's *t*-test). (**c**) Intracellular GSH content of 4T1 or 67NR cells (left), CD44v$^+$ or CD44v$^-$ 4T1 cells (middle), and shC CD44v$^+$ or shESRP1 CD44v$^+$ cells (right). Data are means±s.d. from five independent experiments. **$P<0.01$ (Student's *t*-test). (**d**) IntegriSense images of lung metastases formed in mice 2 weeks after intravenous injection of CD44v$^+$ cells (1×10^5) and the onset of treatment with sulfasalazine or saline. The fluorescence signal intensity of each lung metastasis was also measured; data are means±s.d. for four animals treated with saline and six animals treated with sulfasalazine. **$P<0.01$ (Student's *t*-test). (**e**) Flow cytometric analysis of human CD44v9 expression on the surface of shESRP1 CD44v$^+$ cells stably expressing human CD44v8-10 or stably transfected with the empty vector (mock). (**f**) Intracellular GSH content of cells transfected as in (**e**). Data are means±s.d. from five independent experiments. **$P<0.01$ (Student's *t*-test). (**g**) Mock-transfected or CD44v8-10-expressing shESRP1 CD44v$^+$ cells were incubated with 500 μM H_2O_2 for 20 min, stained with DCFH-DA, and subjected to flow cytometric analysis. Mock-transfected shESRP1 CD44v$^+$ (Mean RFI; 232.73±4.89), CD44v8-10-expressing shC CD44v$^+$ (Mean RFI; 160.19±8.82**). Mean±s.d. values of RFI from five independent experiments. **$P<0.01$ (Student's *t*-test). (**h**) IntegriSense images of lung metastases formed 30 days after orthotopic injection of cells (1×10^5) transfected as in (**e**) into the mammary gland of recipient mice. The fluorescence signal intensity of each lung metastasis was also measured; data are means±s.d. for five animals per group. **$P<0.01$ (Student's *t*-test).

undergoing the epithelial-mesenchymal transition (EMT)[40]. To investigate the relevance of EMT status to ESRP1 expression in CD44v$^+$ and CD44v$^-$ 4T1 cells, we examined the expression of EMT markers and Twist, an EMT-inducing transcription factor that is highly expressed in 4T1 cells[41]. Immunoblot analysis showed that both CD44v$^+$ and CD44v$^-$ cells express the epithelial markers E-cadherin and ZO-1 and that the expression level of Twist was similar in the two cell subpopulations (Fig. 5a), suggesting that ESRP1 expression in CD44v$^+$ and CD44v$^-$ 4T1 cells is regulated independently of EMT-related mechanisms.

Posttranscriptional modifications of histones that affect chromatin structure influence ESRP1-mediated alternative splicing[42,43], suggesting that alternative splicing is tightly regulated at the chromatin level. We therefore examined whether ESRP1 expression might also be regulated epigenetically through histone modification by performing chromatin immunoprecipitation (ChIP) sequencing analysis of the *ESRP1* locus in CD44v$^+$ and CD44v$^-$ cells. CD44v$^+$ cells manifested a marked increase in the amount of trimethylated lysine-4 of histone H3 (H3K4me3), which marks open chromatin and active transcription[44], compared with CD44v$^-$ cells (Fig. 5b). Conversely, the amount of trimethylated lysine-27 of histone H3 (H3K27me3), which is associated with gene silencing[45], was increased in CD44v$^-$ cells (Fig. 5b). Consistent with these histone profiles, RNA polymerase II was enriched at the *ESRP1* locus

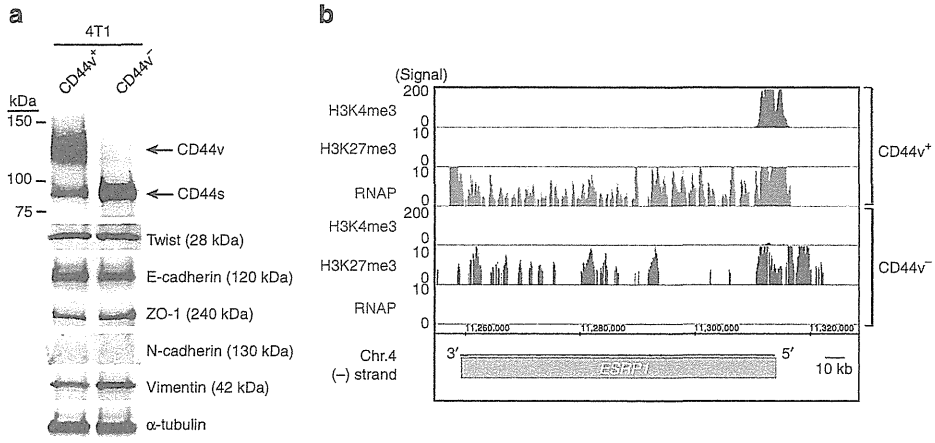

Figure 5 | EMT marker expression and epigenetic status of the *ESRP1* locus in CD44v$^+$ or CD44v$^-$ 4T1 cells. (**a**) Immunoblot analysis of the epithelial markers (E-cadherin and ZO-1) and the mesenchymal markers (N-cadherin and Vimentin) and Twist expression in CD44v$^+$ or CD44v$^-$ 4T1 cells. α-Tubulin was analysed as a loading control. (**b**) Enrichment of histone H3K4me3 and H3K27me3 as well as of RNA polymerase II (RNAP) at the *ESRP1* locus on mouse chromosome 4 in CD44$^+$ or CD44$^-$ 4T1 cells as visualized with the 390-kbp UCSC mm9 genome browser. The gene is transcribed from right to left.

in CD44v$^+$ cells compared with CD44v$^-$ cells (Fig. 5b). Together, these findings suggested that ESRP1 expression in metastatic cancer cells is controlled at the chromatin level.

Discussion

Alternative splicing generates multiple mRNAs from a single-gene transcript, thereby greatly expanding proteomic diversity. Although only a small number of cell type-specific splicing regulators have been identified in mammals, numerous additional regulators will likely be found among the large number of uncharacterized RNA-binding proteins. ESRPs regulate the splicing of transcripts for epithelial- or mesenchymal-specific isoforms of proteins including CD44, FGFR2, p120 catenin, and Mena[14]. The expression of CD44v but not CD44s has been shown to promote the aggressive behaviour in several types of cancer cells including pancreatic cancer[10,46] and lymphoma[47]. We have now shown that depletion of ESRP1 in metastatic breast cancer cells changed the phenotype of these cells from CD44v$^+$ to CD44s$^+$, without affecting the overall level of CD44 expression on the cell surface, and resulted in the suppression of lung metastasis. Consistent with these results, a high expression level of *ESRP1* in tumour specimens was associated with a poor prognosis in breast cancer patients.

Metastasis allows cancer cells to avoid oxidative damage caused by excess ROS in the primary tumour[48], with metastatic cancer cells often being required to adapt to the selective pressure of the tumour microenvironment[19]. Neutrophils were recently shown to accumulate in the lung before the arrival of metastatic cells as well as to inhibit lung metastasis of 4T1 cells through NADPH-dependent H_2O_2 generation[21]. Neutralization of such oxidative stress at potential sites of metastasis may thus be required for cancer cells to establish metastatic lesions.

The cystine transporter xCT promotes GSH synthesis and ROS defence in cancer cells and thereby has a key role in resistance to cancer therapy[18,27], and it has recently been implicated in cancer metastasis[49]. We found that ESRP1-dependent alternative splicing of CD44 mRNA increases both the intracellular GSH level and lung metastatic potential in breast cancer cells. Furthermore, forced expression of CD44v8-10 in ESRP1-depleted cells restored GSH content and lung metastatic ability to levels observed in ESRP1-replete cells. ESRP1-regulated alternative splicing of CD44 mRNA thus enhances xCT-dependent ROS defence and thereby allows cancer cells to evade metastatic stress.

ALDH activity, in addition to CD44 expression, has been shown to be a marker for stem-like cells in breast cancer[38]. ALDH^{high}CD44$^+$ cells among human breast cancer cell lines show increased tumour formation and lung colonization abilities compared with ALDH^{low}CD44$^{low/-}$ cells[6]. We found that both CD44v$^+$ and CD44v$^-$ 4T1 cell subpopulations contain a small number of ALDEFLUOR-positive stem-like cells but that these stem-like cells among the CD44v$^+$ subpopulation underwent selective expansion in lung metastases. CD44v may therefore not be a specific marker for stem-like cancer cells but rather may be required to protect stem-like cells against oxidative stress.

Induction of the EMT results in downregulation of ESRP1 expression[40] and thereby triggers a CD44 isoform switch from CD44v to CD44s in mammary epithelial cells[14,50]. Given that CD44v$^+$ and CD44v$^-$ 4T1 cells manifest similar expression levels of both epithelial and mesenchymal markers, the expression of ESRP1 as well as that of CD44v in these cells do not seem to be dependent on EMT status. ChIP sequencing analysis at the *ESRP1* locus revealed that CD44v$^+$ cells manifest H3K4me3 (a mark of active transcription) at the transcription start site, whereas CD44v$^-$ cells manifest H3K27me3 (a mark of transcriptional repression). ESRP1 expression may thus be affected by the epigenetic status of the *ESRP1* locus as well as by the EMT.

Chromatin modifications including DNA and histone methylation at metastasis-related genes have been considered potential targets for the treatment of cancer metastasis[51]. Therapies targeted to the epigenetic regulation of *ESRP1* as well as those that target CD44v-mediated stabilization of xCT might be expected to perturb the ROS resistance of metastatic stem-like cancer cells and thereby to render them susceptible to currently available cancer treatments.

Methods

Cell culture. The murine breast cancer cell line 4T1 (American Type Culture Collection, Rockville, MD) as well as CD44v$^+$ and CD44v$^-$ cells sorted therefrom were cultured under 5% CO_2 at 37 °C in RPMI 1640 medium (Sigma, St. Louis, MO) supplemented with 10% fetal bovine serum. 67NR, 168FARN, and 4T07 cells (kindly provided by Link Genomics, Tokyo, Japan) were cultured under 5% CO_2 at 37 °C in Dulbecco's modified Eagle's medium-F12 (Sigma) supplemented with 10% fetal bovine serum.

Mice. Wild-type Balb/c mice were obtained from CLEA Japan or Japan SLC (Tokyo, Japan). They were bred and maintained in the animal facility at Keio University according to institutional guidelines. All animal experiments were performed in accordance with protocols approved by the Ethics Committee of Keio University.

Orthotopic transplantation and metastasis assay. Parental, CD44v$^+$, or CD44v$^-$ 4T1 cells (1×10^5) were orthotopically injected into the fourth mammary gland of syngeneic 8-to-10-week-old female wild-type Balb/c mice. At 30 days after transplantation, the mice were killed and the lungs removed. Quantification of lung metastasis was performed by imaging as described below.

IntegriSense imaging. Twenty-four hours before imaging, mice were injected intravenously with 2 nmol of IntegriSense 750 (VisEn Medical, Bedford, MA). Fluorescence imaging was performed with a ClairvivoOPT in vivo fluorescence imager (Shimadzu), with excitation at 785 nm with a laser diode and detection of fluorescence with an 845/55-nm band-pass filter. For quantitative comparisons, the total fluorescence signal intensity (pixel count) in a region of interest corresponding to each lung metastasis was measured.

Tumour cell isolation and flow cytometry. 4T1PT or 4T1LM cells were isolated from primary tumours or lung metastases, respectively, formed 30 days after orthotopic injection of 4T1 cells (1×10^5) into the mammary gland of recipient mice. Primary tumours or lung metastases were digested for 4 to 5 h at 37 °C in Ham's F12 medium supplemented with 5% fetal bovine serum, penicillin (100 U ml^{-1}), streptomycin (100 μg ml^{-1}), bovine insulin (5 μg ml^{-1}), collagenase (300 U ml^{-1}), and hyaluronidase (100 U ml^{-1}). Red blood cells were then lysed by the addition of NH_4Cl to a final concentration of 100 mM at room temperature, and tissue fragments were dissociated by gentle pipetting first in the presence of 0.25% trypsin for 1 to 2 min and then in the additional presence of dispase (5 mg ml^{-1}) and DNase I (0.1 mg ml^{-1}) for 2 min. All reagents were obtained from Stemcell Technologies (Vancouver, Canada). The mixture was then filtered through a 40-μm nylon mesh to yield a single-cell suspension, and the cells were cultured in the presence of 0.4 μM 6-TG (Sigma) for 2 to 3 days and then subjected to FACS to isolate Lin$^-$ cells. Cultured cells were dissociated by exposure to enzyme-free, Hanks-based Cell Dissociation Buffer (GIBCO-Invitrogen, Tokyo, Japan). For flow cytometric analysis or FACS, single-cell suspensions were incubated with antibodies for 20 min at 4 °C. Antibodies included phycoerythrin- and Cy7-conjugated antibodies to the lineage markers (Lin) CD31, CD45, and TER119 (BioLegend, San Diego, CA, USA), phycoerythrin-conjugated antibodies to pan-CD44 (IM7; eBioscience, San Diego, CA, USA), antibodies to xCT (Abcam, Cambridge, UK), allophycocyanin-conjugated antibodies specific for mouse CD44v[52] and fluorescein isothiocyanate-conjugated antibodies to human CD44v9 (ref. 18). Apoptotic cells were excluded for all flow cytometric analysis and FACS by elimination of cells positive for staining with propidium iodide. Flow cytometric analysis and FACS were performed with a FACSCalibur instrument (BD Biosciences, Tokyo, Japan) and either a FACSAria Cell Sorter (BD Biosciences) or MoFlo Cell Sorter (Beckman Coulter, Tokyo, Japan), respectively. For measurement of ROS or GSH levels, cells were incubated with 10 μM DCFH-DA or CFMDA (Invitrogen/Molecular Probes, Tokyo, Japan), respectively, for 15 min at 37 °C, washed twice with phosphate-buffered saline, and subjected to flow cytometric analysis.

Immunoblot analysis. Immunoblot analysis was performed, as described previously[53], and with primary antibodies including those to pan-CD44 (IM7; BD Pharmingen, Tokyo, Japan; 500× dilution), E-cadherin (BD Pharmingen; 1,000× dilution), ZO-1, (Invitrogen, Tokyo, Japan; 1000× dilution), Twist (H-81; Santa Cruz Biotechnology, Santa Cruz, CA, USA; 200× dilution), N-cadherin (N-19; Santa Cruz; 1,000× dilution), Vimentin (BD Pharmingen; 200× dilution), and α-Tubulin (Sigma; 1,000× dilution).

ALDEFLUOR assay. An ALDEFLUOR kit (StemCell Technologies) was used to detect cells with a high ALDH activity. Cells were suspended in ALDEFLUOR assay buffer containing the ALDH substrate BODIPY aminoacetaldehyde (BAAA) and incubated for 40 min at 37 °C. As a negative control, cells were incubated in the additional presence of diethylaminobenzaldehyde (DEAB), a specific ALDH inhibitor.

Imaging mass spectrometry. 4T1 lung metastasis tissues snap-frozen in liquid nitrogen were dissected to prepare cryosections with 5-μm thickness by use of a cryostat (CM 1900; Leica Microsystems, Wetzlar, Germany). The sections were thaw-mounted on indium–tin oxide slides (Bruker Daltonik GmbH, Bremen, Germany) and were dried in silica gel-containing plastic tubes and, then, sprayed with 9-aminoacridine (9-AA, 20 mg in 4 ml 70% MeOH) by use of a 0.2-mm nozzle calibre airbrush (Procon boy FWA Platinum; Mr Hobby, Tokyo, Japan) to conduct matrix-assisted laser desorption/ionization (MALDI) imaging mass spectrometry in negative ion mode[34,35]. Adjacent sections were fixed with 4% buffered formalin (Nacalai Tesque, Kyoto, Japan) and stained with anti-CD44v antibody[52]. All the MALDI imaging experiments was carried out in negative-ion mode using a prototype Mass Microscope (Shimadzu Corporation, Kyoto, Japan). The laser power was adjusted to the desired intensities. MALDI mass spectra were acquired under the conditions laser diameter 10 μm, 80 shots per spot, scanning pitch 10 μm and scanning mass range from m/z 260 to m/z 670. Regions of the tissue samples exposed to the laser irradiation were determined by light microscopic observation.

GSEA. To detect overlap in gene expression profiles among multiple sets of genes, we used GSEA with the Kolmogorov-Smirnov enrichment algorithm and 400 random permutations to determine statistical significance. We first generated CD44v$^+$/CD44v$^-$ $\log_2$ ratio data from our microarray experiment and divided genes into those whose expression was upregulated ($\log_2$ ratio >0) or downregulated ($\log_2$ ratio <0). Second, we collected public microarray data (GSE11274 and GSE16925) from the GEO database and calculated the P-value (t test) and $\log_2$ ratio for ES cells/MEFs or iPS cells/MEFs with the use of the SAM R-package. We extracted the genes with a >2.0-fold change in expression (upregulated) or <0.5-fold change (downregulated) on average and a SAM P-value of <0.05. Third, up- or down-regulated gene sets in our CD44v$^+$/CD44v$^-$ microarray experiment were compared with the ES and iPS cell signature gene sets by GSEA.

ChIP sequencing and data analysis. ChIP was performed as previously described[54]. CD44v$^+$ or CD44v$^-$ 4T1 cells were fixed with 1% formaldehyde, neutralized with 0.2 M glycine, and suspended in a lysis buffer containing 10 mM Tris–HCl (pH 8.0), 150 mM NaCl, 1% SDS, 1 mM EDTA, and a protease inhibitor cocktail (Roche, Tokyo, Japan). The cell lysates were subjected to ultrasonic treatment (Sonifier 250; Branson, Kanagawa, Japan) and diluted with a solution containing 20 mM Tris–HCl (pH 8.0), 150 mM NaCl, 1 mM EDTA, and 1% Triton X-100) for immunoprecipitation with Protein A/G (Invitrogen)-bound antibodies to H3K4me3 or to RNA polymerase II (both kindly provided by H. Kimura) or with those to H3K27me3 (Merck, Tokyo, Japan). Precipitated DNA was prepared according to the Illumina/Solexa Genomic DNA protocol (Illumina, San Diego, CA). The DNA was amplified by PCR (18 cycles) with annealing to the flow cell of a Genome Analyzer. DNA fragments of 350 to 450 bp were purified after separation on an agarose gel and diluted to 10 nM for loading on the flow cell. The DNA library (2 pM) was applied to the flow cell with the use of the Cluster Station device (Illumina). ChIP sequencing (ChIP-seq) data were analysed, as described[54]. In brief, images acquired from the Illumina/Solexa sequencer were processed through the bundled Solexa image extraction pipeline, which identified Polony positions, performed base-calling, and generated quality control (QC) statistics. Sequences were aligned with the human genome in the NCBI genomic database (UCSC mm9) as the reference genome. Sequences that mapped uniquely to the genome with two-base mismatches were selected. Sequences from all lanes for each ChIP sample were combined, extended 200 bp (maximum fragment length accounting for ~100 bp of primer sequence), and allocated into 25-bp bins. Genomic bins showing statistically significant ChIP-seq enrichment were identified by comparison with a Poissonian background model. For every 500-bp (for H3K4me3 and RNA polymerase II) or 1,000-bp (for H3K27me3) window, the mapped tag count for the ChIP sample (C_c) and that for the ChIP input (C_i) were used for calculation. E_c and E_i represent the estimated counts for 500-bp windows for the ChIP sample and ChIP input, respectively. The signal ratio was calculated as $(C_c/E_c+1)/\mathrm{Max}(1, C_i/E_i+1)$. These signals were visualized with Integrated Genome Browser software (Affymetrix, Santa Clara, CA, USA)[55].

Statistical analysis. Data are presented as means±s.d. and were analysed with the unpaired Student's t test. A P-value of <0.05 was considered statistically significant.

References

1. Weigelt, B., Peterse, J. L. & van 't Veer, L. J. Breast cancer metastasis: markers and models. *Nat. Rev. Cancer* **5,** 591–602 (2005).
2. Fidler, I. J. The biology of cancer metastasis. *Semin. Cancer Biol.* **21,** 71 (2011).
3. Mehlen, P. & Puisieux, A. Metastasis: a question of life or death. *Nat. Rev. Cancer* **6,** 449–458 (2006).
4. Liu, H. *et al.* Cancer stem cells from human breast tumors are involved in spontaneous metastases in orthotopic mouse models. *Proc. Natl Acad. Sci. USA* **107,** 18115–18120 (2010).
5. Chaffer, C. L. & Weinberg, R. A. A perspective on cancer cell metastasis. *Science* **331,** 1559–1564 (2011).
6. Croker, A. K. *et al.* High aldehyde dehydrogenase and expression of cancer stem cell markers selects for breast cancer cells with enhanced malignant and metastatic ability. *J. Cell. Mol. Med.* **13,** 2236–2252 (2009).
7. Al-Hajj, M., Wicha, M. S., Benito-Hernandez, A., Morrison, S. J. & Clarke, M. F. Prospective identification of tumorigenic breast cancer cells. *Proc. Natl Acad. Sci. USA* **100,** 3983–3988 (2003).
8. Collins, A. T., Berry, P. A., Hyde, C., Stower, M. J. & Maitland, N. J. Prospective identification of tumorigenic prostate cancer stem cells. *Cancer Res.* **65,** 10946–10951 (2005).
9. Dalerba, P. *et al.* Phenotypic characterization of human colorectal cancer stem cells. *Proc. Natl Acad. Sci. USA* **104,** 10158–10163 (2007).
10. Gunthert, U. *et al.* A new variant of glycoprotein CD44 confers metastatic potential to rat carcinoma cells. *Cell* **65,** 13–24 (1991).
11. Yu, Q., Toole, B. P. & Stamenkovic, I. Induction of apoptosis of metastatic mammary carcinoma cells *in vivo* by disruption of tumor cell surface CD44 function. *J.Exp. Med.* **186,** 1985–1996 (1997).
12. Nagano, O. & Saya, H. Mechanism and biological significance of CD44 cleavage. *Cancer Sci.* **95,** 930–935 (2004).
13. Ponta, H., Sherman, L. & Herrlich, P. A. CD44: from adhesion molecules to signalling regulators. *Nat. Rev. Mol. Cell Biol.* **4,** 33–45 (2003).

14. Warzecha, C. C., Sato, T. K., Nabet, B., Hogenesch, J. B. & Carstens, R. P. ESRP1 and ESRP2 are epithelial cell-type-specific regulators of FGFR2 splicing. *Mol. Cell* **33,** 591–601 (2009).
15. Screaton, G. R., Bell, M. V., Bell, J. I. & Jackson, D. G. The identification of a new alternative exon with highly restricted tissue expression in transcripts encoding the mouse Pgp-1 (CD44) homing receptor. Comparison of all 10 variable exons between mouse, human, and rat. *J. Biol. Chem.* **268,** 12235–12238 (1993).
16. Bennett, K. L. *et al.* CD44 isoforms containing exon V3 are responsible for the presentation of heparin-binding growth factor. *J. Cell Biol.* **128,** 687–698 (1995).
17. Orian-Rousseau, V., Chen, L., Sleeman, J. P., Herrlich, P. & Ponta, H. CD44 is required for two consecutive steps in HGF/c-Met signaling. *Genes Dev.* **16,** 3074–3086 (2002).
18. Ishimoto, T. *et al.* CD44 variant regulates redox status in cancer cells by stabilizing the xCT subunit of system xc(−) and thereby promotes tumor growth. *Cancer Cell* **19,** 387–400 (2011).
19. Chiang, A. C. & Massague, J. Molecular basis of metastasis. *N. Engl. J. Med.* **359,** 2814–2823 (2008).
20. Gupta, G. P. & Massague, J. Cancer metastasis: building a framework. *Cell* **127,** 679–695 (2006).
21. Granot, Z. *et al.* Tumor entrained neutrophils inhibit seeding in the premetastatic lung. *Cancer Cell* **20,** 300–314 (2011).
22. Sato, H. *et al.* Redox imbalance in cystine/glutamate transporter-deficient mice. *J. Biol. Chem.* **280,** 37423–37429 (2005).
23. Huang, Y., Dai, Z., Barbacioru, C. & Sadee, W. Cystine-glutamate transporter SLC7A11 in cancer chemosensitivity and chemoresistance. *Cancer Res.* **65,** 7446–7454 (2005).
24. Calvert, P., Yao, K. S., Hamilton, T. C. & O'Dwyer, P. J. Clinical studies of reversal of drug resistance based on glutathione. *Chem. Biol. Interact.* **111–112,** 213–224 (1998).
25. Goto, S. *et al.* Augmentation of transport for cisplatin-glutathione adduct in cisplatin-resistant cancer cells. *Cancer Res.* **55,** 4297–4301 (1995).
26. Bannai, S. & Ishii, T. Transport of cystine and cysteine and cell growth in cultured human diploid fibroblasts: effect of glutamate and homocysteate. *J. Cell. Physiol.* **112,** 265–272 (1982).
27. Lo, M., Wang, Y. Z. & Gout, P. W. The x(c)− cystine/glutamate antiporter: a potential target for therapy of cancer and other diseases. *J. Cell. Physiol.* **215,** 593–602 (2008).
28. Heppner, G. H., Miller, F. R. & Shekhar, P. M. Nontransgenic models of breast cancer. *Breast Cancer Res.* **2,** 331–334 (2000).
29. Ishimoto, T. *et al.* $CD44^+$ slow-cycling tumor cell expansion is triggered by cooperative actions of Wnt and prostaglandin E2 in gastric tumorigenesis. *Cancer Sci.* **101,** 673–678 (2010).
30. Motohara, T. *et al.* Transient depletion of p53 followed by transduction of c-Myc and K-Ras converts ovarian stem-like cells into tumor-initiating cells. *Carcinogenesis* **32,** 1597–1606 (2011).
31. Subramanian, A. *et al.* Gene set enrichment analysis: a knowledge-based approach for interpreting genome-wide expression profiles. *Proc. Natl Acad. Sci. USA* **102,** 15545–15550 (2005).
32. Ben-Porath, I. *et al.* An embryonic stem cell-like gene expression signature in poorly differentiated aggressive human tumors. *Nat. Genet.* **40,** 499–507 (2008).
33. Pawitan, Y. *et al.* Gene expression profiling spares early breast cancer patients from adjuvant therapy: derived and validated in two population-based cohorts. *Breast Cancer Res.* **7,** R953–R964 (2005).
34. Kubo, A. *et al.* Semi-quantitative analyses of metabolic systems of human colon cancer metastatic xenografts in livers of superimmunodeficient NOG mice. *Anal. Bioanal. Chem.* **400,** 1895–1904 (2011).
35. Morikawa, T. *et al.* Hypoxic regulation of the cerebral microcirculation is mediated by a carbon monoxide-sensitive hydrogen sulfide pathway. *Proc. Natl Acad. Sci. USA* **109,** 1293–1298 (2012).
36. Griffith, O. W. & Meister, A. Potent and specific inhibition of glutathione synthesis by buthionine sulfoximine (S-n-butyl homocysteine sulfoximine). *J. Biol. Chem.* **254,** 7558–7560 (1979).
37. Diehn, M. *et al.* Association of reactive oxygen species levels and radioresistance in cancer stem cells. *Nature* **458,** 780–783 (2009).
38. Ginestier, C. *et al.* ALDH1 is a marker of normal and malignant human mammary stem cells and a predictor of poor clinical outcome. *Cell Stem Cell* **1,** 555–567 (2007).
39. Gout, P. W., Buckley, A. R., Simms, C. R. & Bruchovsky, N. Sulfasalazine, a potent suppressor of lymphoma growth by inhibition of the x(c)− cystine transporter: a new action for an old drug. *Leukemia* **15,** 1633–1640 (2001).
40. Warzecha, C. C. *et al.* An ESRP-regulated splicing programme is abrogated during the epithelial-mesenchymal transition. *EMBO J.* **29,** 3286–3300 (2010).
41. Yang, J. *et al.* Twist, a master regulator of morphogenesis, plays an essential role in tumor metastasis. *Cell* **117,** 927–939 (2004).
42. Saint-Andre, V., Batsche, E., Rachez, C. & Muchardt, C. Histone H3 lysine 9 trimethylation and HP1gamma favor inclusion of alternative exons. *Nat. Struct. Mol. Biol.* **18,** 337–344 (2011).
43. Wagner, E. J. & Carpenter, P. B. Understanding the language of Lys36 methylation at histone H3. *Nat. Rev. Mol. Cell. Biol.* **13,** 115–126 (2012).
44. Guenther, M. G., Levine, S. S., Boyer, L. A., Jaenisch, R. & Young, R. A. A chromatin landmark and transcription initiation at most promoters in human cells. *Cell* **130,** 77–88 (2007).
45. Cao, R. *et al.* Role of histone H3 lysine 27 methylation in Polycomb-group silencing. *Science* **298,** 1039–1043 (2002).
46. Klingbeil, P. *et al.* CD44 variant isoforms promote metastasis formation by a tumor cell-matrix cross-talk that supports adhesion and apoptosis resistance. *Mol. Cancer Res.* **7,** 168–179 (2009).
47. Wallach-Dayan, S. B. *et al.* CD44-dependent lymphoma cell dissemination: a cell surface CD44 variant, rather than standard CD44, supports *in vitro* lymphoma cell rolling on hyaluronic acid substrate and its *in vivo* accumulation in the peripheral lymph nodes. *J. Cell. Sci.* **114,** 3463–3477 (2001).
48. Pani, G., Galeotti, T. & Chiarugi, P. Metastasis: cancer cell's escape from oxidative stress. *Cancer Metastasis Rev.* **29,** 351–378 (2010).
49. Chen, R. S. *et al.* Disruption of xCT inhibits cancer cell metastasis via the caveolin-1/beta-catenin pathway. *Oncogene* **28,** 599–609 (2009).
50. Brown, R. L. *et al.* CD44 splice isoform switching in human and mouse epithelium is essential for epithelial-mesenchymal transition and breast cancer progression. *J. Clin. Invest.* **121,** 1064–1074 (2011).
51. Sahin, M., Sahin, E., Gumuslu, S., Erdogan, A. & Gultekin, M. DNA methylation or histone modification status in metastasis and angiogenesis-related genes: a new hypothesis on usage of DNMT inhibitors and S-adenosylmethionine for genome stability. *Cancer Metastasis Rev.* **29,** 655–676 (2010).
52. Ishimoto, T. *et al.* $CD44^+$ slow-cycling tumor cell expansion is triggered by cooperative actions of Wnt and prostaglandin E2 in gastric tumorigenesis. *Cancer Sci.* **101,** 673–678 (2010).
53. Nagano, O. *et al.* Cell-matrix interaction via CD44 is independently regulated by different metalloproteinases activated in response to extracellular Ca^{2+} influx and PKC activation. *J. Cell Biol.* **165,** 893–902 (2004).
54. Tozawa, H. *et al.* Genome-wide approaches reveal functional interleukin-4-inducible STAT6 binding to the vascular cell adhesion molecule 1 promoter. *Mol. Cell. Biol.* **31,** 2196–2209 (2011).
55. Nicol, J. W., Helt, G. A., Blanchard, S. G. Jr., Raja, A. & Loraine, A. E. The integrated genome browser: free software for distribution and exploration of genome-scale datasets. *Bioinformatics* **25,** 2730–2731 (2009).

Acknowledgements

We thank I. Ishimatsu, S.Suzuki, S.Hayashi, Y.Hata and K.Hizume for technical assistance; K.Arai for help in preparation of the manuscript. O.N. and H.S. are grateful to A.Izumi-Taguchi, T.Kodama (Lab for Systems Biology and Medicine, Research Center for Advanced Science and Technology, University of Tokyo, Meguro-Ku, Tokyo 153-8904, Japan), H.Ueda, T.Miyazawa, S.Yamamoto, K.Shiina and G.Nagae (Genome Science Division, Research Center for Advanced Science and Technology, University of Tokyo) for technical assistance in ChIP-sequencing analysis. Antibodies against Histone H3K4me3, Pol II were kindly provided by H.Kimura (Graduate School of Frontier Biosciences, Osaka University, Suita, Osaka 565-0871, Japan). This work was supported by grants from the Ministry of Education, Culture, Sports, Science, and Technology of Japan (to H.S.) as well as in part by the Project for Development of Innovative Research on Cancer Therapeutics (P-Direct), Ministry of Education, Culture, Sports, Science and Technology of Japan(to O.N.). Imaging mass spectrometry analysis was supported by Grant-in-Aid from the SENTAN Program from JST and Development of the Next-Generation Integrated Simulation of Living Matter, a Part of Development and Use of the Next-Generation Supercomputer Project of MEXT Japan.

Author contributions

H.S., K. Takahashi, and O.N. conceived the project and designed experiments. T.Y., K. Tsuchihashi, T.I., T. Motohara, M.Y., G. J. Y., T.W., T.O., Y.K., and A.K. performed experiments. T. Masuko, K.M., H.T., T. Minami, H.A., M.O. and M.S. analysed the data. H.S. and O.N. wrote the manuscript.

Additional information

Accession codes: The microarray data have been deposited in the GEO database under the accession code GSE35803.

Supplementary Information accompanies this paper at http://www.nature.com/naturecommunications

Competing financial interests: The authors declare no competing financial interests.

Reprints and permission information is available online at http://npg.nature.com/reprintsandpermissions/

How to cite this article: Yae, T. *et al.* Alternative splicing of *CD44* mRNA by ESRP1 enhances lung colonization of metastatic cancer cell. *Nat. Commun.* 3:883 doi: 10.1038/ncomms1892 (2012).

DOI:10.1158/1078-0432.CCR-12-0859

Clinical Cancer Research

Pyruvate Kinase M2: Multiple Faces for Conferring Benefits on Cancer Cells

Mayumi Tamada, Makoto Suematsu and Hideyuki Saya

Clin Cancer Res 2012;18:5554-5561. Published online October 14, 2012.

DOI:10.1158/1078-0432.CCR-12-0859

Pyruvate Kinase M2: Multiple Faces for Conferring Benefits on Cancer Cells

Mayumi Tamada[1], Makoto Suematsu[2,4], and Hideyuki Saya[1,3]

Abstract

The M2 splice isoform of pyruvate kinase (PKM2), an enzyme that catalyzes the later step of glycolysis, is a key regulator of aerobic glycolysis (known as the Warburg effect) in cancer cells. Expression and low enzymatic activity of PKM2 confer on cancer cells the glycolytic phenotype, which promotes rapid energy production and flow of glycolytic intermediates into collateral pathways to synthesize nucleic acids, amino acids, and lipids without the accumulation of reactive oxygen species. PKM2 enzymatic activity has also been shown to be negatively regulated by the interaction with CD44 adhesion molecule, which is a cell surface marker for cancer stem cells. In addition to the glycolytic functions, nonglycolytic functions of PKM2 in cancer cells are of particular interest. PKM2 is induced translocation into the nucleus, where it activates transcription of various genes by interacting with and phosphorylating specific nuclear proteins, endowing cancer cells with a survival and growth advantage. Therefore, inhibitors and activators of PKM2 are well underway to evaluate their anticancer effects and suitability for use as novel therapeutic strategies. *Clin Cancer Res; 18(20); 5554–61. ©2012 AACR.*

Introduction

Obtaining sufficient energy is a critical issue for cells to survive. Regardless of local availability of molecular oxygen, mainly cancer cells primarily use glycolysis to produce ATP. This unique feature is called aerobic glycolysis or the Warburg effect (1, 2). Recent studies show that pyruvate kinase M2 (PKM2) is a key glycolytic enzyme that regulates the Warburg effect and is necessary for tumor growth (3). Incorporated glucose is converted into pyruvate through several steps in cytoplasm (Fig. 1). Pyruvate can be converted to lactate or to acetyl-CoA, and such direction is determined by the enzymatic activity of PKM2 (3–6). Low PKM2 activity promotes conversion to lactate and leads to Warburg effect, whereas high activity of both PKM2 and PKM1 promotes conversion to acetyl-CoA (Fig. 1; refs. 3–6). Recently, not only the glycolytic but also the nonglycolytic functions of PKM2 have attracted a great deal of attention. In this review, we describe the functions of PKM2 in cancer cells and discuss potential therapeutic applications.

Authors' Affiliations: [1]Division of Gene Regulation, Institute for Advanced Medical Research, School of Medicine, [2]Department of Biochemistry, School of Medicine, Keio University; [3]Japan Science and Technology Agency, Core Research for Evolutional Science and Technology (CREST); and [4]Japan Science and Technology Agency, Exploratory Research for Advanced Technology (ERATO), Suematsu Gas Biology Project, Tokyo, Japan

Corresponding Author: Hideyuki Saya, Division of Gene Regulation, Institute for Advanced Medical Research, School of Medicine, Keio University, 35 Shinanomachi, Shinjuku-ku, Tokyo 160-8582, Japan. Phone: 81-3-5363-3982; Fax: 81-3-5363-3982; E-mail: hsaya@a5.keio.jp

doi: 10.1158/1078-0432.CCR-12-0859

Four Isoforms of Pyruvate Kinase

Pyruvate kinase (PK) is a glycolytic enzyme that catalyzes a reaction generating pyruvate and ATP from phosphoenolpyruvate (PEP) and ADP (Fig. 1). Four isoforms of PK (L, R, M1, and M2) are present in mammals. The L and R isotypes are encoded by the *PKLR* gene. Their expression is tissue specific and is regulated by different promoters. The L isotype is expressed in the liver, kidney, and intestine, and the R isotype is expressed in red blood cells (7–10). PKM1 and PKM2 are encoded by the *PKM* gene and are the products of 2 mutually exclusive alternatively spliced exons (exon 9 and exon 10, respectively; refs. 7, 11, 12): M1 is expressed in most adult differentiated tissues such as brain and muscle, whereas M2 is expressed in embryonic cells, adult stem cells, and cancer cells (3, 8, 9, 13–15). Splicing of *PKM* is controlled by the splicing repressors, heterogeneous nuclear ribonucleoprotein (hnRNP) A1 and A2, as well as polypyrimidine tract binding protein (PTB, also known as hnRNPI), and the expression of those repressors is upregulated by MYC oncoprotein (Fig. 2; refs. 7, 11). These proteins bind to exon 9 and repress *PKM1* mRNA splicing, resulting in the inclusion of exon 10 and thereby contributing to the high levels of PKM2 expression (7, 11, 16).

PKM2 Expression in Cancer Cells

In addition to embryonic cells and adult stem cells, PKM2 is a major isoform expressed in cancer cells (3, 8, 9, 13–15). The expression of PKM2 is necessary for tumor growth (3, 15, 17–20) and a number of regulators of PKM2 expression have been reported (7, 8, 11, 16, 21–23). A recent study showed that PKM2 expression is induced by activated mTOR, which transactivates hypoxia-inducible factor 1 (HIF-1) and promotes the c-Myc-hnRNPs–mediated

DOI:10.1158/1078-0432.CCR-12-0859

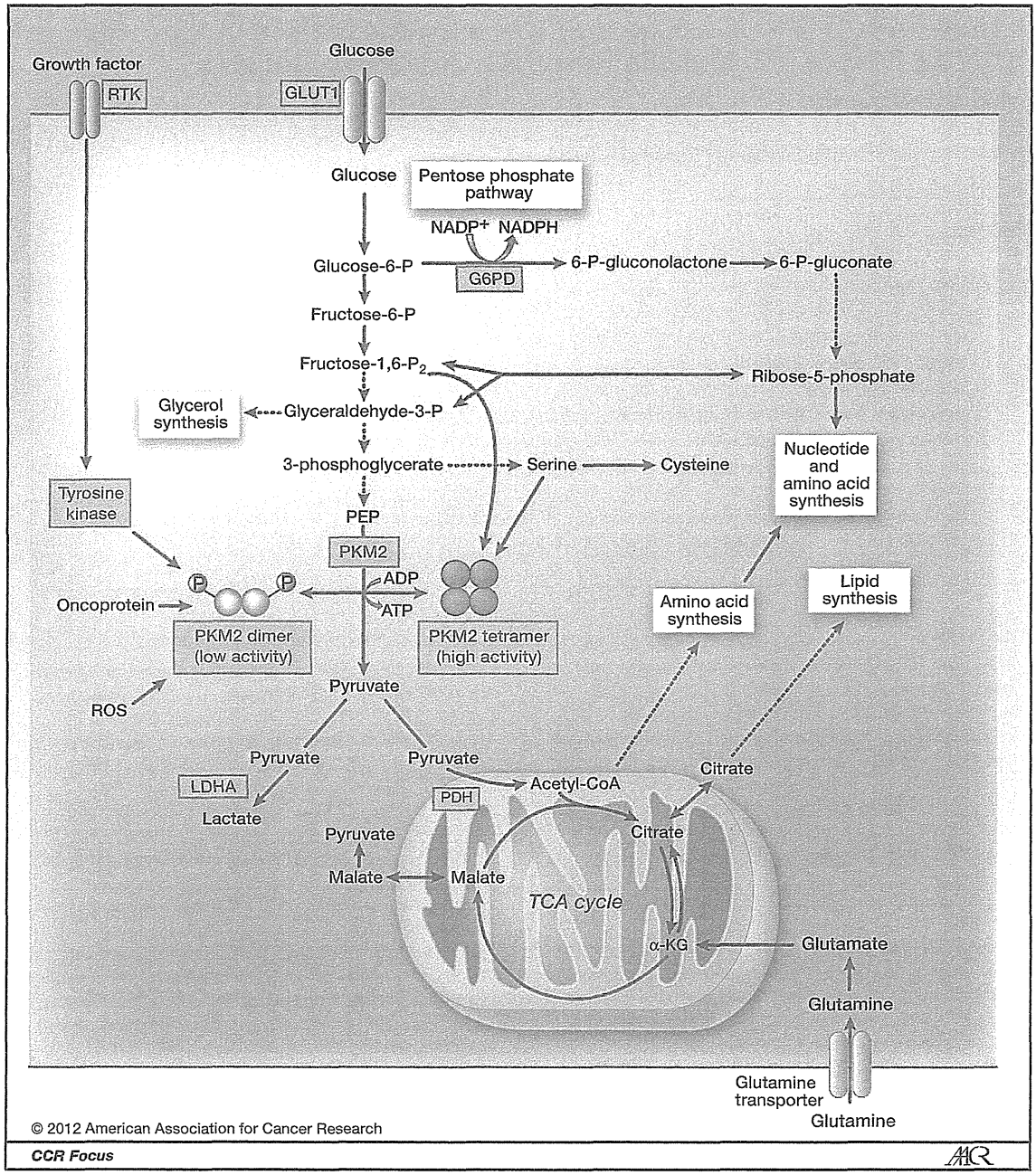

Figure 1. Metabolic pathway regulated by PKM2 in cancer cells. PKM2 exists in both a low-activity dimeric form and a high-activity tetrameric form. The less active dimeric form of PKM2 is phosphorylated by tyrosine kinases and promotes the conversion of pytuvate to lactate. In contrast, the high-activity tetrameric form promotes the conversion of pyruvate to acetyl-CoA. Intermediates of glycolysis can also enter other collateral pathways, where they are used to synthesize nucleotides, glycerol, and NADPH. G6PD, glucose-6-phosphate dehydrogenase; ROS, reactive oxygen species; RTK, receptor tyrosine kinase; TCA, tricarboxylic acid.

alternative splicing, leading to the aerobic glycolysis in tumor cells (24).

Enhanced expression of PKM2 is observed both in various cancer cell lines and in samples such as blood, serum, and stool from cancer patients (3, 9, 15, 25–27). Given that the upregulation of PKM2, concomitant with the downregulation of PKM1, is induced in skin cells within 24 hours of treatment with the tumor promoter,

DOI:10.1158/1078-0432.CCR-12-0859

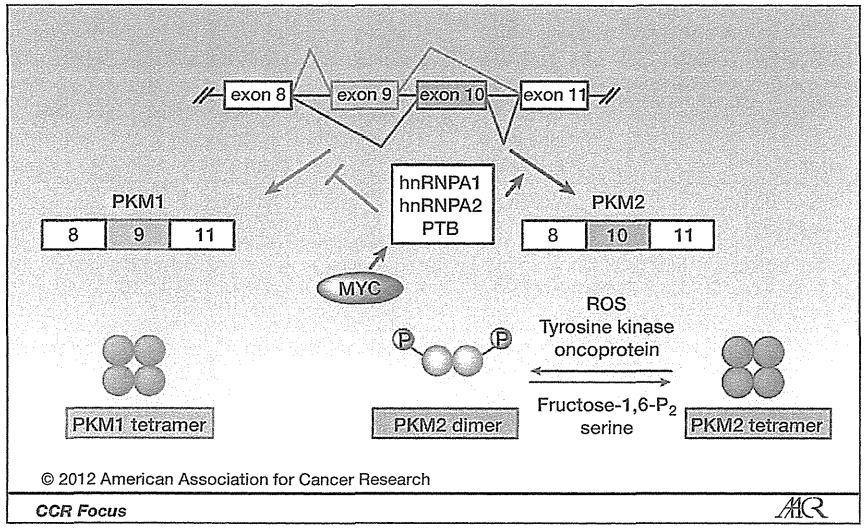

Figure 2. PKM1 and PKM2 expression after alternative splicing. The alternative exons, which encode the different segments of PKM1 and PKM2, are indicated in blue (exon 9) and red (exon 10) boxes. Mutually exclusive alternative splicing of exon 9 and exon 10 is indicated. HnRNP proteins (hnRNPA1 and hnRNPA2) and PTB (also known as hnRNPI) controlled by MYC bind to exon 9 and repress *PKM1* mRNA splicing, resulting in the inclusion of exon 10, forming *PKM2* mRNA. PKM2 exists in 2 oligomeric forms: a high-activity tetrameric form and a low-activity dimeric form, whereas PKM1 constitutively exists as high-activity tetrameric form. Several factors affect the switch between the dimeric and tetrameric forms. Oncoproteins, tyrosine kinase–mediated phosphorylation, and oxidative stress all promote the formation of the low-activity dimer. In contrast, fructose-1,6-P_2 and serine promote the reverse situation. hnRNP, heterogeneous nuclear ribonucleoprotein.

12-O-tetradecanoylphorbol-13-acetate, PKM2 expression might be an early event in carcinogenesis (28). Thus, PKM2 can be a useful biomarker for the early detection of tumors.

Glycolytic Functions of PKM2

The expression and lower glycolytic enzyme activity of PKM2 are necessary for the Warburg effect, which provides cancer cells with selective advantages, including tumor growth and suppression of reactive oxygen species (ROS; refs. 3, 4, 15, 18) for the following 2 reasons. First is that the glycolytic pathway generates ATP more rapidly than the oxidative phosphorylation (29), allowing faster incorporation of carbon into its biomass (4, 30). Between yield and rate of ATP production, a trade-off has been reported to be present in sugar degradation by glycolysis and mitochondrial respiration. Then, glycolysis generates ATP at a high rate but low yield via massive consumption of glucose (29, 31). The second reason is that lower activity of PKM2 facilitates the production of glycolytic intermediates to enter the glycolysis branch pathways, such as glycerol synthesis and the pentose phosphate pathway, which generates NADPH to suppress ROS production and is also involved in nucleotide synthesis (Fig. 1; refs. 4, 15, 30, 32, 33). In other words, the increase in glycolysis induced by the lower activity of PKM2 can supply cancer cells with varied resources of substrates necessary for their rapid proliferation.

PKM2 exists as either a low-activity dimeric or high-activity tetrameric form, whereas PKM1 constantly exists as a high-activity tetrameric form (Figs. 1 and 2; refs. 8, 9, 34). Cancer cells predominantly express the low-activity dimeric form of PKM2 (3, 5, 6), whereas normal proliferating cells express the high-activity tetrameric form (9). Christofk and colleagues (3) and Vander Heiden and colleagues (35) from Cantley's group reported that PKM1-expressing cells showed much higher PK activity than PKM2-expressing cells; these cells consumed more oxygen, produced less lactate, and were highly sensitive to the mitochondrial ATP synthesis inhibitor, oligomycin (3). In addition, Hitosugi and colleagues reported that tyrosine phosphorylation (Tyr 105) of PKM2 disrupts the active tetrameric form of PKM2, leading to the suppression of its activity. Furthermore, PKM2-mutated cells, in which tyrosine residue 105 is replaced with a phenylalanine, had increased PK activity as observed in PKM1-expressing cells (6). Therefore, the low activity of dimeric PKM2 is a very important driver for glycolysis. In contrast, the high activity of PKM2 and PKM1 tetramers drives the tricarboxylic acid (TCA) cycle (Figs. 1 and 2; refs. 3–6).

Various factors have been reported to control the switch between the dimeric and tetrameric forms of PKM2 (5, 6, 8, 19, 36–44). For example, fructose-1,6-bisphosphate (fructose-1,6-P_2), a glycolytic intermediate, binds allosterically to PKM2 and facilitates the formation of the active tetramer. Serine, which is produced from a glycolytic intermediate 3-phosphoglycerate, is also a positive regulator of PKM2 (Figs. 1 and 2A; refs. 8, 45–48). In contrast, tyrosine phosphorylation of PKM2 induces the release of fructose-1,6-P_2, which causes PKM2 to convert from tetrameric form to less active dimeric form (5, 6). In addition, oncoproteins such as HPV-16 E7 and activated $pp60^{v\text{-}src}$ kinase dissociate the tetrameric form to yield the dimeric form (49).

DOI:10.1158/1078-0432.CCR-12-0859

Furthermore, recent studies show that oxidative stress causes dissociation of the tetramer and a subsequent reduction in PKM2 activity (Figs. 1 and 2; ref. 18), and that acetylation of lysine residue within PKM2 suppresses its catalytic activity and induces the degradation by chaperone-mediated autophagy (22). In addition, it has been reported that mucin 1 phosphorylated by EGF receptor (EGFR) interacts with PKM2 and suppresses its activity (50).

Nonglycolytic Functions of PKM2

A variety of molecules interact with PKM2 (5, 6, 8, 14, 18, 19, 21, 23, 24, 28, 36–45, 50–65). Many of them affect the glycolytic functions of PKM2, which directly regulate the Warburg effect. However, an increasing number of reports document the nonglycolytic functions of PKM2. In particular, the role of PKM2 in transcription is attracting attention. It has been reported that PKM2 interacts directly with the HIF-1 subunit and promotes transactivation of HIF-1 target genes (Fig. 3; ref. 21). As HIF-1 also activates the transcription of the genes encoding PKM2, cancer cells may have the positive feedback loop between PKM2 and HIF-1, which contributes to the characteristic metabolism in cancer cells.

There have been several studies about PKM2 nuclear translocation. It is induced not only by such events as interleukin-3 stimulation and EGFR activation, which relate to cell proliferation (19, 52), but also by apoptotic stimuli such as somatostatin analogues, hydrogen peroxide (H_2O_2), and UV light (58). Nuclear PKM2 has been shown to activate gene transcriptions and cell proliferation (14, 19–21, 52, 61). Translocation of PKM2 into the nucleus induced by EGFR activation was reported to promote β-catenin transactivation, leading to expression of cyclinD1 and c-Myc (Fig. 3; ref. 52). Given that c-Myc upregulates transcription of hnRNPs contributing to the high PKM2/PKM1 ratio (7, 11), and that c-Myc promotes glycolysis by driving the expression of glucose transporter1 (GLUT1) and lactate dehydrogenase A (66, 67), the events induced by the

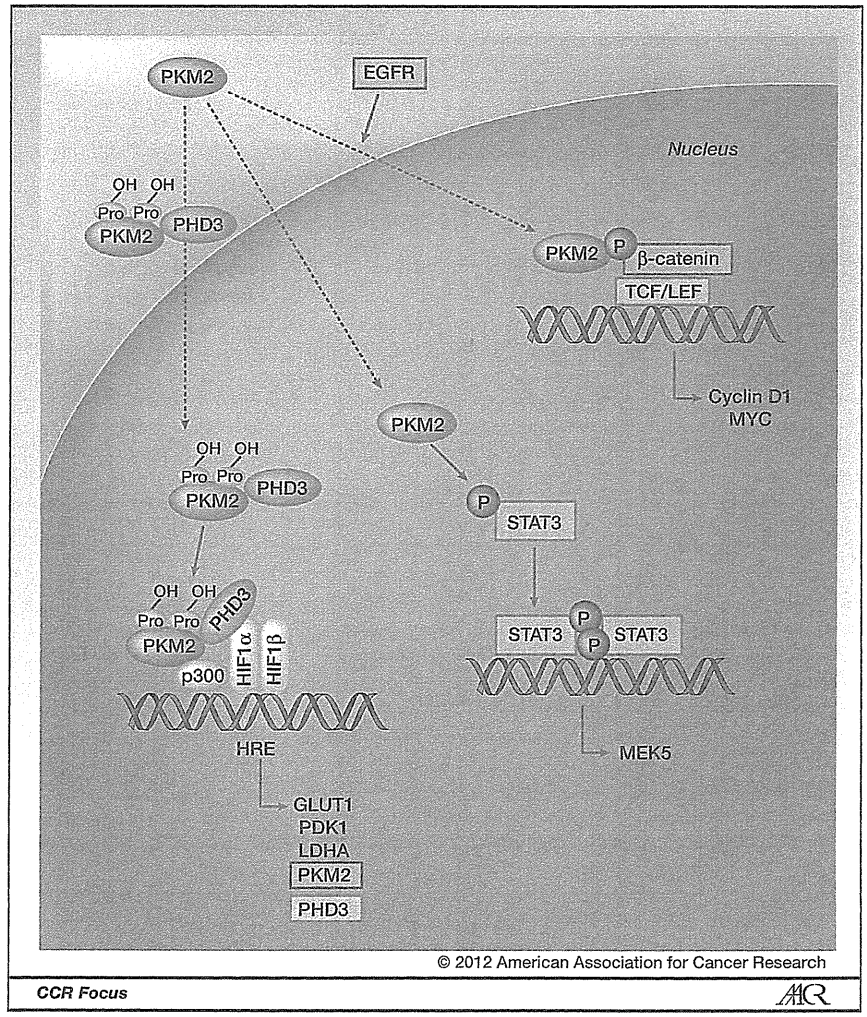

CCR Focus

Figure 3. Representative nonglyclolytic functions of PKM2 in the nucleus. PHD3-dependent prolyl hydroxylated PKM2 interacts with HIF-1 and p300, enhancing HIF-1 to occupy HRE of the target genes. Nuclear-PKM2 functions as an active protein kinase capable of phosphorylating STAT3. Phosphorylated STAT3 activates *Mek5* transcription via increasing its DNA-binding ability. EGFR activation induces translocation of PKM2 into the nucleus. PKM2-β-catenin complex, together with TCF/LEF, promotes expression Cyclin D1 and c-MYC. HRE, hypoxia response element; PDK1, pyruvate dehydrogenase kinase 1; PHD, prolyl hydroxylase domain.

DOI:10.1158/1078-0432.CCR-12-0859

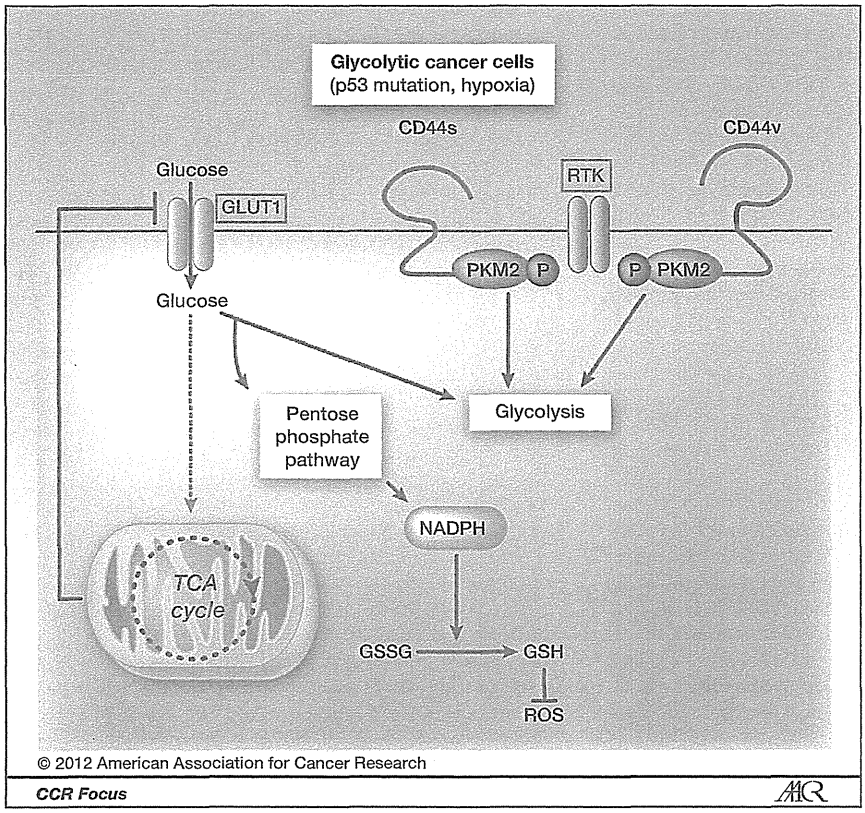

Figure 4. Schematic diagram of CD44/PKM2 interaction-regulating GSH production in glycolytic cancer cells. The CD44/PKM2 interaction suppresses PKM2 activity via tyrosine phosphorylation and promotes glycolysis. Promotion of glycolysis and suppression of the TCA cycle are maintained by the CD44/PKM2 interaction, which is related to increased glucose uptake mediated by upregulated GLUT1. Increasing glucose uptake and subsequent PPP flux that produces NADPH contribute to increased GSH production and reduced ROS accumulation. CD44s, standard isoform of CD44, which lacks all variant exons; CD44v, splice variant isoforms of CD44, which contain variable exons; GSH, glutathione; RTK, receptor tyrosine kinase.

translocation of PKM2 into the nucleus may be connected with a feed-forward loop to drive glycolysis.

Nuclear PKM2 has been reported to exist as a dimeric form, whereas cytoplasmic PKM2 exists as both dimeric and tetrameric form (20). In addition, the nuclear PKM2 was shown to act as a protein kinase that can phosphorylate STAT3 and thereby activate transcription of cancer-relevant genes such as *Mek5* (Fig. 3; ref. 20). Taking these findings together, we speculate that PKM2 has 2 faces for conferring great benefits on cancer cells. First is that dimeric PKM2 in cytoplasm acts as a PK in which enzymatic activity is low for maintaining the glycolytic phenotype and promoting glycolytic intermediates to a collateral pathway for biosynthesis. The second is that the dimeric PKM2 translocated in the nucleus acts as an active protein kinase to phosphorylate specific nuclear proteins. Recently, many other roles of PKM2 in various conditions such as immunologic responses (43, 44, 63, 64), genomic instability (37), angiogenesis (57), pathogenesis (36, 41, 62), and some disease (54) have been reported. It is important to define whether those events are associated with glycolytic or nonglycolytic functions of PKM2.

PKM2 and the Management of Oxidative Stress

CD44 is a major adhesion molecule and a cell surface marker for cancer stem cells. CD44 has been shown to be implicated in tumorigenesis as well as tumor growth and metastasis (51, 68, 69). Recently, we found that CD44 interacts with PKM2. The CD44/PKM2 interaction suppresses PKM2 enzymatic activity via tyrosine phosphorylation, thereby promoting glycolysis and increasing the flux to the pentose phosphate pathway (PPP) in glycolytic cancer cells that are either p53 dysfunctional or hypoxic (Fig. 4; ref. 51). CD44 ablation enhances mitochondrial respiration through metabolic shift from glycolysis, which may suppress GLUT1 expression, thereby reducing glucose uptake, and subsequent PPP flux. Such metabolic changes induced by CD44 ablation lead to the downregulation of reduced glutathione (GSH) synthesis in cells, along with a consequent increase in ROS accumulation (Fig. 4; ref. 51). Interestingly, PKM2 activity is inhibited by oxidative stress as well as tyrosine phosphorylation (18). Oxidative stress induces the oxidization of Cys358 within PKM2, which promotes glycolysis and PPP flux, leading to the production of GSH and consequent ROS depletion (18, 70, 71). Thus, cancer cells have multiple mechanisms for avoiding ROS accumulation, which gives them a survival advantage in terms of tumor growth and therapeutic resistance (18, 51, 72).

Therapeutic Possibilities for PKM2

Cancer-specific metabolism, which is associated with therapeutic resistance, is an attractive target for cancer

DOI:10.1158/1078-0432.CCR-12-0859

therapy (30, 66, 67, 73–78). As outlined above, PKM2 plays many important roles in metabolism and signals in cancer cells and, thereby, can be an ideal therapeutic target. The RNA interference and the peptide aptamers which ablate PKM2 have been reported to elicit anticancer effects, such as the impairment of tumor growth, induction of apoptotic cell death, and increasing sensitivity to chemotherapy (3, 17, 56, 79, 80). Small-molecule inhibitors of PKM2 have already been identified, and these inhibitors suppress glycolysis and cause cell death. However, therapies targeting PKM2 expression are problematic. One problem is that PKM2 is also expressed in some normal tissues (8). The other is that PKM2 knockdown by short hairpin RNA does not completely disrupt cancer cell proliferation; nevertheless, it induces near-complete depletion of PKM2 activity (77). Thus, the compounds that activate the catalytic function of PKM2 may have a role as therapeutic modalities (32, 33, 77, 81). Given that the activity of PKM2 expressed in normal tissues is high, whereas that in cancer cells is low (9), such activators may inhibit glycolysis and proliferation in cancer cells with less toxic effects in normal cells. PKM2 activators show a similar effect of fructose-1,6-P_2, which induces tetrameric formation of PKM2 (33). Because nucleic PKM2 exists as a dimer, PKM2 activators have a potential to prevent PKM2 from moving into the nucleus and thereby suppress functions of nucleic PKM2. In other words, PKM2 activators may be capable of inhibiting both glycolytic and nonglycolytic functions of PKM2.

Inhibition of glycolytic function of PKM2 can suppress glycolysis, leading to an increase in ROS production and a decreasing supply of varied resources of substrates necessary for rapid cancer cell proliferation. Inhibition of nonglycolytic function of PKM2 can suppress the activation of cancer-relevant genes such as *Mek5*, *c-Myc*, and various HIF-1 target genes (Fig. 3). Further studies are required to ensure their suitability for cancer therapy.

Our group reported that CD44 ablation increases the enzyme activity of PKM2, thereby inducing metabolic changes, including a shift from glycolysis to TCA cycle, leading to suppression of glucose uptake mediated down-regulation of GLUT1 expression (51). Such metabolic changes induced by CD44 ablation reduce the flux to PPP and consequently accumulate ROS (Fig. 4). This sensitizes glycolytic cancer cells such as p53-mutated cells and hypoxic cells to anticancer drugs. Thus, our data suggest that indirect activation of PKM2 may have a synergistic effect when used in combination with existing therapies.

Conclusions and Future Directions

Both the glycolytic and nonglycolytic functions of PKM2 provide cancer cells with growth and survival advantages. PKM2 expression was shown to be involved in early tumorigenesis (28) and can be detected in the blood and stool of cancer patients (9, 82); furthermore, increases in PKM2 levels were reported to correlate with tumor size and stage (9). As described in another article in this *CCR Focus* section by Yang and colleagues, mutations of IDH1 and IDH2 are also reported to be easily detectable using small amounts of tumor samples (83). Accordingly, these enzymes involved in cancer metabolism can be useful biomarkers.

It was recently shown that the microenvironment also confers metabolic heterogeneity on cancer tissues (15, 77). Such metabolic heterogeneity may be caused by the differences in the supply of nutrients and oxygen because each cancer cell is located at a different distance from the blood vessels (77). Acetylation of PKM2, which inhibits its catalytic activity, is triggered by high glucose levels (22, 30, 84). PKM2 acts as a metabolic sensor in a manner that is dependent upon the glucose supply (79). The regulation of HIF-1 and PKM2 also differs according to the degree of hypoxia (21, 85). In addition, Hamanaka and colleagues suggested that PKM2 inhibitors suppress ATP production under severely hypoxic conditions; however, PKM2 activators would increase oxidative damage under moderately hypoxic conditions (30). Interestingly, PKM2-overexpressing stromal cells have been reported to supply recycled chemical building blocks such as lipids or nucleotides via autophagy, increase ketone body secretion, and fuel mitochondrial respiration of adjacent cancer cells (86).

In conclusion, the status of PKM2 is regulated by both intrinsic and extrinsic factors. Through the glycolytic and nonglycolytic functions, PKM2 contributes to the malignant phenotype of cancer cells, suggesting it could be an excellent target for cancer therapy. However, PKM2 has multiple faces and the intracellular events elicited by PKM2 are far more complicated than previously assumed. Furthermore, the effects of targeting PKM2 on normal cells have not been fully assessed. Therefore, further studies are needed before inhibitors and activators of PKM2 can be used as therapeutic interventions.

Disclosure of Potential Conflicts of Interest

H. Saya, commercial research grants, Kyowa Hakko Kirin Co. Ltd and Daiichi Sankyo Co. Ltd. No potential conflicts of interest were disclosed by the other authors.

Authors' Contributions

Conception and design: M. Tamada, H. Saya
Development of methodology: M. Tamada
Acquisition of data (provided animals, acquired and managed patients, provided facilities, etc.): M. Tamada
Analysis and interpretation of data (e.g., statistical analysis, biostatistics, computational analysis): M. Tamada
Writing, review, and/or revision of the manuscript: M. Tamada, M. Suematsu, H. Saya
Administrative, technical, or material support (i.e., reporting or organizing data, constructing databases): M. Tamada

Acknowledgments

The authors thank members of the division of Gene Regulation, IAMR, School of Medicine, Keio University, for their important suggestions, and K. Arai for help with preparation of the manuscript.

Grant Support

This work was supported in part by a Grant-in-Aid for Scientific Research from the Ministry of Education, Culture, Sports, Science and Technology (MEXT), Japan (H. Saya), and the Global COE Program, MEXT, Japan (M. Tamada).

Received May 25, 2012; revised July 26, 2012; accepted August 28, 2012; published online October 15, 2012.

DOI:10.1158/1078-0432.CCR-12-0859

References

1. Warburg O, Wind F, Negelein E. The metabolism of tumors in the body. J Gen Physiol 1927;8:519–30.
2. Gatenby RA, Gillies RJ. Why do cancers have high aerobic glycolysis? Nat Rev 2004;4:891–9.
3. Christofk HR, Vander Heiden MG, Harris MH, Ramanathan A, Gerszten RE, Wei R, et al. The M2 splice isoform of pyruvate kinase is important for cancer metabolism and tumour growth. Nature 2008;452:230–3.
4. Vander Heiden MG, Cantley LC, Thompson CB. Understanding the Warburg effect: the metabolic requirements of cell proliferation. Science 2009;324:1029–33.
5. Christofk HR, Vander Heiden MG, Wu N, Asara JM, Cantley LC. Pyruvate kinase M2 is a phosphotyrosine-binding protein. Nature 2008;452:181–6.
6. Hitosugi T, Kang S, Vander Heiden MG, Chung TW, Elf S, Lythgoe K, et al. Tyrosine phosphorylation inhibits PKM2 to promote the Warburg effect and tumor growth. Sci Signal 2009;2:ra73.
7. Clower CV, Chatterjee D, Wang Z, Cantley LC, Vander Heiden MG, Krainer AR. The alternative splicing repressors hnRNP A1/A2 and PTB influence pyruvate kinase isoform expression and cell metabolism. Proc Natl Acad Sci U S A 2010;107:1894–9.
8. Mazurek S. Pyruvate kinase type M2: a key regulator of the metabolic budget system in tumor cells. Int J Biochem Cell Biol 2011;43:969–80.
9. Mazurek S, Boschek CB, Hugo F, Eigenbrodt E. Pyruvate kinase type M2 and its role in tumor growth and spreading. Semin Cancer Biol 2005;15:300–8.
10. Noguchi T, Yamada K, Inoue H, Matsuda T, Tanaka T. The L- and R-type isozymes of rat pyruvate kinase are produced from a single gene by use of different promoters. J Biol Chem 1987;262:14366–71.
11. David CJ, Chen M, Assanah M, Canoll P, Manley JL. HnRNP proteins controlled by c-Myc deregulate pyruvate kinase mRNA splicing in cancer. Nature 2010;463:364–8.
12. Noguchi T, Inoue H, Tanaka T. The M1- and M2-type isozymes of rat pyruvate kinase are produced from the same gene by alternative RNA splicing. J Biol Chem 1986;261:13807–12.
13. Bluemlein K, Gruning NM, Feichtinger RG, Lehrach H, Kofler B, Ralser M. No evidence for a shift in pyruvate kinase PKM1 to PKM2 expression during tumorigenesis. Oncotarget 2011;2:393–400.
14. Lee J, Kim HK, Han YM, Kim J. Pyruvate kinase isozyme type M2 (PKM2) interacts and cooperates with Oct-4 in regulating transcription. Int J Biochem Cell Biol 2008;40:1043–54.
15. Cairns RA, Harris IS, Mak TW. Regulation of cancer cell metabolism. Nat Rev 2011;11:85–95.
16. Chen M, David CJ, Manley JL. Concentration-dependent control of pyruvate kinase M mutually exclusive splicing by hnRNP proteins. Nat Struct Mol Biol 2012;19:346–54.
17. Goldberg MS, Sharp PA. Pyruvate kinase M2-specific siRNA induces apoptosis and tumor regression. J Exp Med 2012;209:217–24.
18. Anastasiou D, Poulogiannis G, Asara JM, Boxer MB, Jiang JK, Shen M, et al. Inhibition of pyruvate kinase M2 by reactive oxygen species contributes to cellular antioxidant responses. Science 2011;334:1278–83.
19. Hoshino A, Hirst JA, Fujii H. Regulation of cell proliferation by interleukin-3-induced nuclear translocation of pyruvate kinase. J Biol Chem 2007;282:17706–11.
20. Gao X, Wang H, Yang JJ, Liu X, Liu ZR. Pyruvate kinase M2 regulates gene transcription by acting as a protein kinase. Mol Cell 2012;45:598–609.
21. Luo W, Hu H, Chang R, Zhong J, Knabel M, O'Meally R, et al. Pyruvate kinase M2 is a PHD3-stimulated coactivator for hypoxia-inducible factor 1. Cell 2011;145:732–44.
22. Lv L, Li D, Zhao D, Lin R, Chu Y, Zhang H, et al. Acetylation targets the M2 isoform of pyruvate kinase for degradation through chaperone-mediated autophagy and promotes tumor growth. Mol Cell 2011;42:719–30.
23. Panasyuk G, Espeillac C, Chauvin C, Pradelli LA, Horie Y, Suzuki A, et al. PPARgamma contributes to PKM2 and HK2 expression in fatty liver. Nat Commun 2012;3:672.
24. Sun Q, Chen X, Ma J, Peng H, Wang F, Zha X, et al. Mammalian target of rapamycin up-regulation of pyruvate kinase isoenzyme type M2 is critical for aerobic glycolysis and tumor growth. Proc Natl Acad Sci U S A 2011;108:4129–34.
25. Luftner D, Mesterharm J, Akrivakis C, Geppert R, Petrides PE, Wernecke KD, et al. Tumor type M2 pyruvate kinase expression in advanced breast cancer. Anticancer Res 2000;20:5077–82.
26. Schneider J, Neu K, Grimm H, Velcovsky HG, Weisse G, Eigenbrodt E. Tumor M2-pyruvate kinase in lung cancer patients: immunohistochemical detection and disease monitoring. Anticancer Res 2002;22:311–8.
27. Cerwenka H, Aigner R, Bacher H, Werkgartner G, el-Shabrawi A, Quehenberger F, et al. TUM2-PK (pyruvate kinase type tumor M2), CA19-9 and CEA in patients with benign, malignant and metastasizing pancreatic lesions. Anticancer Res 1999;19:849–51.
28. Wittwer JA, Robbins D, Wang F, Codarin S, Shen X, Kevil CG, et al. Enhancing mitochondrial respiration suppresses tumor promoter TPA-induced PKM2 expression and cell transformation in skin epidermal JB6 cells. Cancer Prevent Res 2011;4:1476–84.
29. Pfeiffer T, Schuster S, Bonhoeffer S. Cooperation and competition in the evolution of ATP-producing pathways. Science 2001;292:504–7.
30. Hamanaka RB, Chandel NS. Targeting glucose metabolism for cancer therapy. J Exp Med 2012;209:211–5.
31. Vazquez A, Liu J, Zhou Y, Oltvai ZN. Catabolic efficiency of aerobic glycolysis: the Warburg effect revisited. BMC Syst Biol 2010;4:58.
32. Jiang JK, Boxer MB, Vander Heiden MG, Shen M, Skoumbourdis AP, Southall N, et al. Evaluation of thieno[3,2-b]pyrrole[3,2-d]pyridazinones as activators of the tumor cell specific M2 isoform of pyruvate kinase. Bioorg Med Chem Lett 2010;20:3387–93.
33. Boxer MB, Jiang JK, Vander Heiden MG, Shen M, Skoumbourdis AP, Southall N, et al. Evaluation of substituted N,N'-diarylsulfonamides as activators of the tumor cell specific M2 isoform of pyruvate kinase. J Med Chem 2010;53:1048–55.
34. Dang CV. PKM2 tyrosine phosphorylation and glutamine metabolism signal a different view of the Warburg effect. Sci Signal 2009;2:pe75.
35. Vander Heiden MG, Locasale JW, Swanson KD, Sharfi H, Heffron GJ, Amador-Noguez D, et al. Evidence for an alternative glycolytic pathway in rapidly proliferating cells. Science 2010;329:1492–9.
36. Wu X, Zhou Y, Zhang K, Liu Q, Guo D. Isoform-specific interaction of pyruvate kinase with hepatitis C virus NS5B. FEBS Lett 2008;582:2155–60.
37. Shimada N, Shinagawa T, Ishii S. Modulation of M2-type pyruvate kinase activity by the cytoplasmic PML tumor suppressor protein. Gens Cells 2008;13:245–54.
38. Mazurek S, Drexler HC, Troppmair J, Eigenbrodt E, Rapp UR. Regulation of pyruvate kinase type M2 by A-Raf: a possible glycolytic stop or go mechanism. Anticancer Res 2007;27:3963–71.
39. Siwko S, Mochly-Rosen D. Use of a novel method to find substrates of protein kinase C delta identifies M2 pyruvate kinase. Int J Biochem Cell Biol 2007;39:978–87.
40. LeMellay V, Houben R, Troppmair J, Hagemann C, Mazurek S, Frey U, et al. Regulation of glycolysis by Raf protein serine/threonine kinases. Adv Enzyme Regul 2002;42:317–32.
41. Zwerschke W, Mazurek S, Massimi P, Banks L, Eigenbrodt E, Jansen-Durr P. Modulation of type M2 pyruvate kinase activity by the human papillomavirus type 16 E7 oncoprotein. Proc Natl Acad Sci U S A 1999;96:1291–6.
42. Presek P, Glossmann H, Eigenbrodt E, Schoner W, Rubsamen H, Friis RR, et al. Similarities between a phosphoprotein (pp60src)-associated protein kinase of Rous sarcoma virus and a cyclic adenosine 3′:5′-monophosphate-independent protein kinase that phosphorylates pyruvate kinase type M2. Cancer Res 1980;40:1733–41.
43. Ryu H, Walker JK, Kim S, Koo N, Barak LS, Noguchi T, et al. Regulation of M2-type pyruvate kinase mediated by the high-affinity IgE receptors is required for mast cell degranulation. Br J Pharmacol 2008;154:1035–46.
44. Zhang Z, Liu Q, Che Y, Yuan X, Dai L, Zeng B, et al. Antigen presentation by dendritic cells in tumors is disrupted by altered metabolism that involves pyruvate kinase M2 and its interaction with SOCS3. Cancer Res 2010;70:89–98.

DOI:10.1158/1078-0432.CCR-12-0859

45. Ward PS, Thompson CB. Metabolic reprogramming: a cancer hallmark even warburg did not anticipate. Cancer Cell 2012;21:297–308.
46. Ashizawa K, Willingham MC, Liang CM, Cheng SY. *In vivo* regulation of monomer-tetramer conversion of pyruvate kinase subtype M2 by glucose is mediated via fructose 1,6-bisphosphate. J Biol Chem 1991;266:16842–6.
47. Eigenbrodt E, Leib S, Kramer W, Friis RR, Schoner W. Structural and kinetic differences between the M2 type pyruvate kinases from lung and various tumors. Biomed Biochim Acta 1983;42:S278–82.
48. Ye J, Mancuso A, Tong X, Ward PS, Fan J, Rabinowitz JD, et al. Pyruvate kinase M2 promotes *de novo* serine synthesis to sustain mTORC1 activity and cell proliferation. Proc Natl Acad Sci U S A 2012;109:6904–9.
49. Mazurek S, Grimm H, Boschek CB, Vaupel P, Eigenbrodt E. Pyruvate kinase type M2: a crossroad in the tumor metabolome. Br J Nutr 2002;87 Suppl 1:S23–9.
50. Kosugi M, Ahmad R, Alam M, Uchida Y, Kufe D. MUC1-C oncoprotein regulates glycolysis and pyruvate kinase M2 activity in cancer cells. PLoS One 2011;6:e28234.
51. Tamada M, Nagano O, Tateyama S, Ohmura M, Yae T, Ishimoto T, et al. Modulation of glucose metabolism by CD44 contributes to antioxidant status and drug resistance in cancer cells. Cancer Res 2012;72:1438–48.
52. Yang W, Xia Y, Ji H, Zheng Y, Liang J, Huang W, et al. Nuclear PKM2 regulates beta-catenin transactivation upon EGFR activation. Nature 2011;480:118–22.
53. Diaz-Jullien C, Moreira D, Sarandeses CS, Covelo G, Barbeito P, Freire M. The M2-type isoenzyme of pyruvate kinase phosphorylates prothymosin alpha in proliferating lymphocytes. Biochim Biophys Acta 2011;1814:355–65.
54. Gupta V, Bamezai RN. Human pyruvate kinase M2: a multifunctional protein. Protein Sci 2010;19:2031–44.
55. Spoden GA, Morandell D, Ehehalt D, Fiedler M, Jansen-Durr P, Hermann M, et al. The SUMO-E3 ligase PIAS3 targets pyruvate kinase M2. J Cell Biochem 2009;107:293–302.
56. Spoden GA, Mazurek S, Morandell D, Bacher N, Ausserlechner MJ, Jansen-Durr P, et al. Isotype-specific inhibitors of the glycolytic key regulator pyruvate kinase subtype M2 moderately decelerate tumor cell proliferation. Int J Cancer 2008;123:312–21.
57. Duan HF, Hu XW, Chen JL, Gao LH, Xi YY, Lu Y, et al. Antitumor activities of TEM8-Fc: an engineered antibody-like molecule targeting tumor endothelial marker 8. J Natl Cancer Inst 2007;99:1551–5.
58. Stetak A, Veress R, Ovadi J, Csermely P, Keri G, Ullrich A. Nuclear translocation of the tumor marker pyruvate kinase M2 induces programmed cell death. Cancer Res 2007;67:1602–8.
59. Li Y, Chang Y, Zhang L, Feng Q, Liu Z, Zhang Y, et al. High glucose upregulates pantothenate kinase 4 (PanK4) and thus affects M2-type pyruvate kinase (Pkm2). Mol Cell Biochem 2005;277:117–25.
60. Garcia-Gonzalo FR, Cruz C, Munoz P, Mazurek S, Eigenbrodt E, Ventura F, et al. Interaction between HERC1 and M2-type pyruvate kinase. FEBS Lett 2003;539:78–84.
61. Ignacak J, Stachurska MB. The dual activity of pyruvate kinase type M2 from chromatin extracts of neoplastic cells. Comp Biochem Physiol B Biochem Mol Biol 2003;134:425–33.
62. Mazurek S, Zwerschke W, Jansen-Durr P, Eigenbrodt E. Effects of the human papilloma virus HPV-16 E7 oncoprotein on glycolysis and glutaminolysis: role of pyruvate kinase type M2 and the glycolytic-enzyme complex. Biochem J 2001;356:247–56.
63. Oak MH, Cheong H, Kim KM. Activation of Fc epsilon RI inhibits the pyruvate kinase through direct interaction with the gamma-chain. Int Arch Allergy Immunol 1999;119:95–100.
64. Williams JM, Chen GC, Zhu L, Rest RF. Using the yeast two-hybrid system to identify human epithelial cell proteins that bind gonococcal Opa proteins: intracellular gonococci bind pyruvate kinase via their Opa proteins and require host pyruvate for growth. Mol Microbiol 1998;27:171–86.
65. Kato H, Fukuda T, Parkison C, McPhie P, Cheng SY. Cytosolic thyroid hormone-binding protein is a monomer of pyruvate kinase. Proc Natl Acad Sci U S A 1989;86:7861–5.
66. Munoz-Pinedo C, El Mjiyad N, Ricci JE. Cancer metabolism: current perspectives and future directions. Cell Death Dis 2012;3:e248.
67. Dang CV, Le A, Gao P. MYC-induced cancer cell energy metabolism and therapeutic opportunities. Clinical Cancer Res 2009;15:6479–83.
68. Nagano O, Saya H. Mechanism and biological significance of CD44 cleavage. Cancer Sci 2004;95:930–5.
69. Visvader JE, Lindeman GJ. Cancer stem cells in solid tumours: accumulating evidence and unresolved questions. Nat Rev 2008;8:755–68.
70. Gruning NM, Ralser M. Cancer: sacrifice for survival. Nature 2011;480:190–1.
71. Hamanaka RB, Chandel NS. Cell biology. Warburg effect and redox balance. Science 2011;334:1219–20.
72. Ishimoto T, Nagano O, Yae T, Tamada M, Motohara T, Oshima H, et al. CD44 variant regulates redox status in cancer cells by stabilizing the xCT subunit of system xc(-) and thereby promotes tumor growth. Cancer cell 2011;19:387–400.
73. Meijer TWH, Kaanders JHAM, Span PN, Bussink J. Targeting hypoxia, HIF-1 and tumor glucose metabolism to improve radiotherapy efficacy. Clin Cancer Res 2012;18:5585–94.
74. Jerby L, Ruppin E. Predicting drug targets and biomarkers of cancer via genome-scale metabolic modeling. Clin Cancer Res 2012;18:5572–84.
75. Dang CV, Hamaker M, Sun P, Le A, Gao P. Therapeutic targeting of cancer cell metabolism. J Mol Med 2011;89:205–12.
76. Iaccarino I, Martins LM. Therapeutic targets in cancer cell metabolism and death. Cell Death Differ 2011;18:565–70.
77. VanderHeiden MG. Targeting cancer metabolism: a therapeutic window opens. Nat Rev Drug Discov 2011;10:671–84.
78. Bonnet S, Archer SL, Allalunis-Turner J, Haromy A, Beaulieu C, Thompson R, et al. A mitochondria-K+ channel axis is suppressed in cancer and its normalization promotes apoptosis and inhibits cancer growth. Cancer Cell 2007;11:37–51.
79. Spoden GA, Rostek U, Lechner S, Mitterberger M, Mazurek S, Zwerschke W. Pyruvate kinase isoenzyme M2 is a glycolytic sensor differentially regulating cell proliferation, cell size and apoptotic cell death dependent on glucose supply. Exp Cell Res 2009;315:2765–74.
80. Guo W, Zhang Y, Chen T, Wang Y, Xue J, Zhang Y, et al. Efficacy of RNAi targeting of pyruvate kinase M2 combined with cisplatin in a lung cancer model. J Cancer Res Clin Oncol 2011;137:65–72.
81. Walsh MJ, Brimacombe KR, Veith H, Bougie JM, Daniel T, Leister W, et al. 2-Oxo-N-aryl-1,2,3,4-tetrahydroquinoline-6-sulfonamides as activators of the tumor cell specific M2 isoform of pyruvate kinase. Bioorg Med Chem Lett 2011;21:6322–7.
82. Hathurusinghe HR, Goonetilleke KS, Siriwardena AK. Current status of tumor M2 pyruvate kinase (tumor M2-PK) as a biomarker of gastrointestinal malignancy. Ann Surg Oncol 2007;14:2714–20.
83. Yang H, Ye D, Guan K-L, Xiong Y. IDH1 and IDH2 mutations in tumorigenesis: mechanistic insights and clinical perspectives. Clin Cancer Res 2012;18:5562–71.
84. Macintyre AN, Rathmell JC. PKM2 and the tricky balance of growth and energy in cancer. Molecular cell 2011;42:713–4.
85. Tennant DA. PK-M2 makes cells sweeter on HIF1. Cell 2011;145:647–9.
86. Chiavarina B, Whitaker-Menezes D, Martinez-Outschoorn UE, Witkiewicz AK, Birbe RC, Howell A, et al. Pyruvate kinase expression (PKM1 and PKM2) in cancer-associated fibroblasts drives stromal nutrient production and tumor growth. Cancer Biol Ther 2011;12:1101–13.

Cell Host & Microbe
Article

Reactive Oxygen Species-Induced Autophagic Degradation of *Helicobacter pylori* CagA Is Specifically Suppressed in Cancer Stem-like Cells

Hitoshi Tsugawa,[1] Hidekazu Suzuki,[1,*] Hideyuki Saya,[2] Masanori Hatakeyama,[3] Toshiya Hirayama,[4] Kenro Hirata,[1] Osamu Nagano,[2] Juntaro Matsuzaki,[1] and Toshifumi Hibi[1]
[1]Division of Gastroenterology and Hepatology, Department of Internal Medicine
[2]Division of Gene Regulation, Institute for Advanced Medical Research
Keio University School of Medicine, Tokyo 160-8582, Japan
[3]Division of Microbiology, Graduate School of Medicine, University of Tokyo, Tokyo 113-0033, Japan
[4]Department of Bacteriology, Institute of Tropical Medicine, Nagasaki University, Nagasaki 852-8523, Japan
*Correspondence: hsuzuki@a6.keio.jp
http://dx.doi.org/10.1016/j.chom.2012.10.014

SUMMARY

Sustained expression of CagA, the type IV secretion effector of *Helicobacter pylori*, is closely associated with the development of gastric cancer. However, we observed that after translocation, CagA is degraded by autophagy and therefore short lived. Autophagy and CagA degradation are induced by the *H. pylori* vacuolating cytotoxin, VacA, which acted via decreasing intracellular glutathione (GSH) levels, causing reactive oxygen species (ROS) accumulation and Akt activation. Investigating this further, we found that CagA specifically accumulated in gastric cells expressing CD44, a cell-surface marker associated with cancer stem cells. The autophagic pathway in CD44-positive gastric cancer stem-like cells is suppressed because of their resistance to ROS, which is supported by increased intracellular GSH levels. These findings provide a molecular link between *H. pylori* and gastric carcinogenesis through the specific accumulation of CagA in gastric cancer stem-like cells.

INTRODUCTION

A possible link has been demonstrated between *Helicobacter pylori* infection and development of gastric cancer by epidemiological (Uemura et al., 2001) and animal studies (Suzuki et al., 2009). Although long-term *H. pylori* infections of the gastric mucosa might cause gastric cancer from severe inflammation, no direct molecular link was demonstrated until Hatakeyama reported that the transfer of *H. pylori*-derived CagA to epithelial cells through a bacterial type IV secretion system promoted an early event of gastric carcinogenesis (Hatakeyama, 2004). Ohnishi et al. (2008) also demonstrated that systemic expression of CagA in *cagA*-transgenic mice induced gastrointestinal malignancies, indicating the oncogenic potential of bacterial CagA in mammals. However, it was also reported that CagA, after translocation to gastric epithelial cells, does not persist for a long period (Ishikawa et al., 2009).

Recently, it has been reported that autophagy—a system for bulk protein degradation and the elimination of invaded pathogens (Deretic and Levine, 2009)—is induced in *H. pylori*-infected cells (Raju et al., 2012; Terebiznik et al., 2009). In the present study, we observed that intracellular CagA was degraded by autophagy induced by the accumulation of reactive oxygen species (ROS), suggesting that CagA may not promote carcinogenesis. Even if CagA escapes the autophagy system, intracellular CagA could never be transferred to daughter cells and would be lost after cell division. If translocated CagA does indeed trigger gastric carcinogenesis, it should be transferred to slow-cycling master-regulator cells and escape from autophagic degradation.

CD44 is a cell-surface marker associated with cancer stem cells in various tumors (Dalerba et al., 2007). Gastric cancer stem-like cells expressing the variant isoform of CD44 (CD44v9) suppress ROS accumulation by control of intracellular glutathione (GSH) levels by stabilizing xCT, a cystine transporter (Ishimoto et al., 2011). In the present report, we used CD44v9-expressing gastric cancer stem-like cells to study the ability of intracellular CagA to escape from autophagy and show a direct molecular link between *H. pylori*-derived CagA and gastric cancer stem-like cells.

RESULTS

CagA Is Degraded by Autophagy

To investigate the stability of intracellular CagA, we constructed an in vitro *H. pylori* infection model using a gastric cancer cell line (AGS). After 5 hr of *H. pylori* ATCC700392 infection, the AGS cells were incubated with kanamycin to kill extracellular bacteria. In AGS cells after *H. pylori* eradication, the levels of intracellular CagA and tyrosine-phosphorylated CagA (p-CagA) decreased in a time-dependent manner (Figure 1A). Therefore, intracellular CagA did not persist for a prolonged period in gastric epithelial cells and was soon degraded by host cell defenses.

To examine the mechanism of CagA degradation in host epithelial cells, we used proteasome inhibitors (MG132 and lactacystin [Lact]) and autophagy inhibitors (3-methyladenine [3MA] and wortmannin [Wort]). At 24 hr after *H. pylori* ATCC700392 eradication, while intracellular CagA and p-CagA levels were

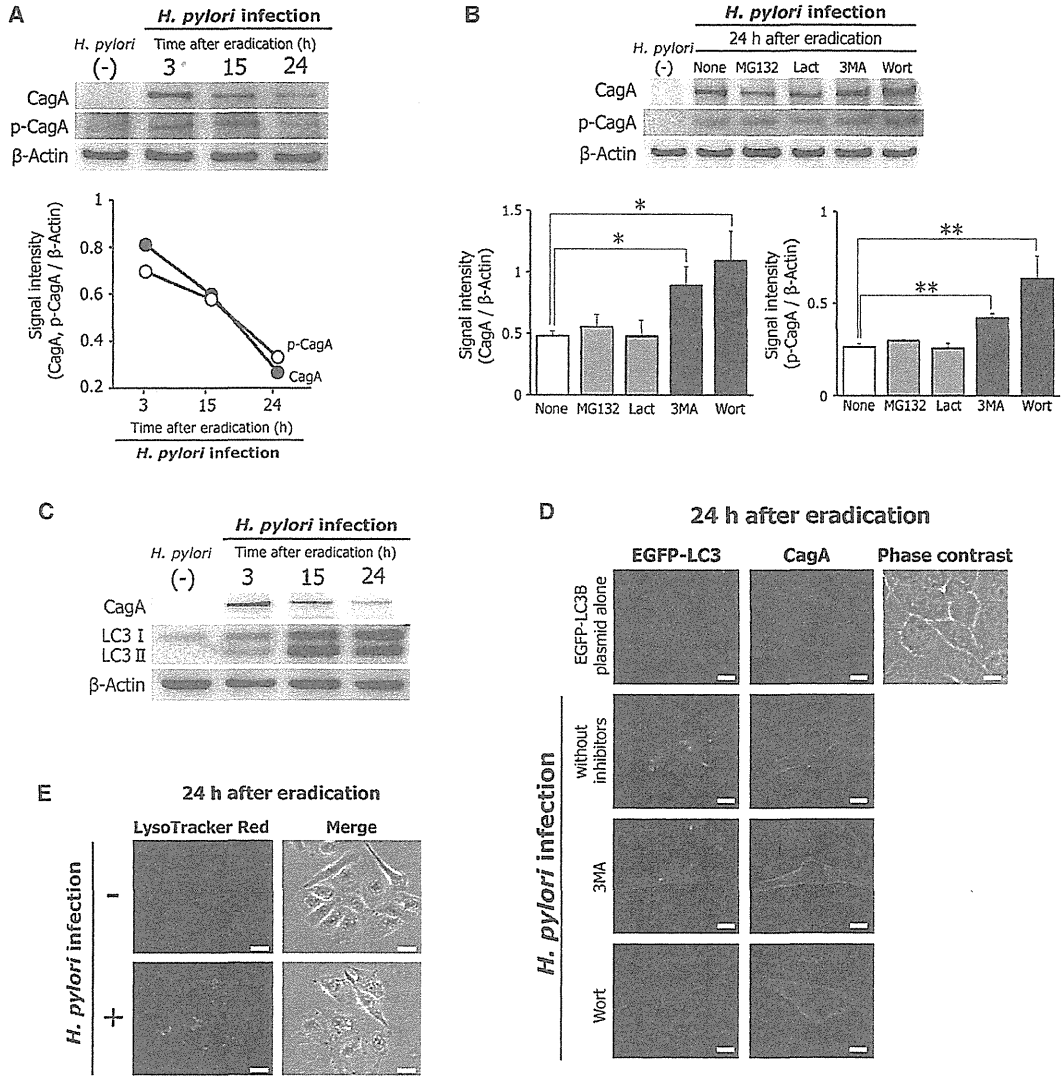

Figure 1. Autophagy Induction Associated with Intracellular CagA Stability

(A) AGS cells infected with *H. pylori* ATCC700392 for 5 hr were incubated at indicated times in a medium containing antibiotic to kill extracellular bacteria. Intracellular CagA and phosphorylated CagA (p-CagA) levels were quantified. Data represent the mean of three independent assays.

(B) AGS cells infected with *H. pylori* for 5 hr were incubated in a medium containing antibiotic with or without a proteasome inhibitor (10 μM MG132 or 20 μM lactacystin [Lact]) or autophagy inhibitor (5 mM 3-methyladenine [3MA] or 50 nM wortmannin [Wort]) for 24 hr. Intracellular CagA and p-CagA levels were quantified. Data represent the mean ± SD of three independent assays; *$p < 0.05$, **$p < 0.01$.

(C) AGS cells infected with *H. pylori* ATCC700392 for 5 hr were incubated in a medium containing antibiotic for the indicated times, and intracellular CagA and LC3-I to LC3-II conversion were examined.

(D) After transfection of AGS cells with the EGFP-LC3B plasmid, cells infected with *H. pylori* for 5 hr were incubated with a medium containing antibiotic for 24 hr with or without an autophagy inhibitor (10 μM MG132 or 20 μM Lact), and intracellular CagA was stained. EGFP-LC3B plasmid alone indicates the absence of *H. pylori* infection. Scale bar = 25 μm.

(E) AGS cells infected with *H. pylori* ATCC700392 for 5 hr were incubated with a medium containing antibiotic for 24 hr, and LysoTracker Red DND-99 staining was performed. Scale bar = 50 μm.

not affected by proteasome inhibitors (10 μM MG132 or 20 μM Lact), they were significantly increased by exposure of the cells to autophagy inhibitors (5 mM 3MA or 50 nM Wort), as compared with cells not exposed to these inhibitors (None) (Figure 1B). These results indicated that autophagy contributed to CagA degradation in host epithelial cells.

We then examined whether autophagy was activated within AGS cells after *H. pylori* ATCC700392 eradication. A hallmark of autophagy is the carboxyl terminus modification of microtubule-associated protein light chain 3 (LC3), which becomes linked to phosphatidylethanolamine and associates with the autophagosomal membrane. LC3-I to LC3-II conversion was

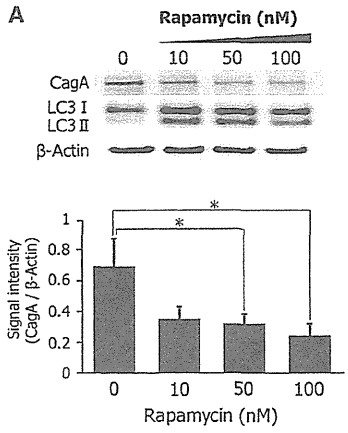

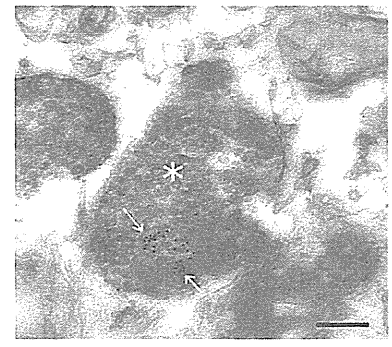

Figure 2. Degradation of Intracellular CagA by the Induction of Autophagy

(A) CagA expression in WT-A10 cells was induced by removal of Dox for 24 hr (CagA-expressing WT-A10 cells). CagA-expressing WT-A10 cells were stimulated with rapamycin for 24 hr, and intracellular CagA and LC3-I to LC3-II conversion were examined. Data represent the mean ± SD of three independent assays; *$p < 0.05$.

(B) CagA-expressing WT-A10 cells stimulated with 100 nM rapamycin for 24 hr were reacted with a 15 nm immunogold-labeled antibody; immunogold-labeled CagA was detected by electron microscopy. Arrows indicate immunogold-labeled CagA. Label is autophagolysosomal components. Scale bar = 200 nm.

detected most clearly at 15 and 24 hr after *H. pylori* eradication (Figure 1C). In addition, 24 hr after eradication, EGFP-LC3B-positive puncta were clearly detected within the cytoplasm of AGS cells transfected with the EGFP-LC3B plasmid, unlike AGS cells exposed to autophagy inhibitors (5 mM 3MA, 50 nM Wort) (Figure 1D), suggesting that LC3 is activated and localized to autophagosomes. LysoTracker Red stains late autophagic vacuoles (autolysosomes), but not early autophagosomes. LysoTracker Red staining was clearly detected within AGS cells at 24 hr after *H. pylori* eradication, consistent with the formation of autolysosomes (Figure 1E). These results demonstrate that autophagy was activated in AGS cells at 15 and 24 hr after eradication.

To evaluate whether autophagy was specifically associated with degradation of intracellular CagA, CagA-expressing WT-A10 cells—in which CagA expression was induced through the pTet-off-*cagA* expression vector by the absence of doxycycline (Dox) for 24 hr—was used. When these cells were incubated with rapamycin, which promotes autophagy by inhibiting mammalian target of rapamycin (mTOR), intracellular CagA decreased in a dose-dependent manner, and LC3-I to LC3-II conversion was clearly detected (Figure 2A). In addition, electron immunocytochemical examination following immunogold labeling for CagA in CagA-expressing, rapamycin-stimulated WT-A10 cells revealed the presence of labeled CagA in autophagic vesicles (Figure 2B). From these results, we conclude that intracellular CagA is degraded by autophagy.

CagA Degradation via Autophagy Is Activated by m1VacA

Although autophagy was activated in AGS cells after *H. pylori* eradication (Figures 1C–1E), no LC3-I to LC3-II conversion was detected in CagA-expressing WT-A10 cells without rapamycin (Figure 2A; rapamycin [0 nM] lane). These results indicate that the induction of autophagy was independent of intracellular CagA, but was dependent on *H. pylori* infection. According to Terebiznik et al. (2009), autophagy was induced by VacA in *H. pylori*-infected AGS cells; therefore, we tested whether VacA participated in induction of autophagy associated with CagA degradation. In CagA-expressing WT-A10 cells exposed to culture supernatant from *H. pylori* ATCC700392 (s1m1VacA), intracellular CagA levels were significantly decreased in the culture supernatant in a dose-dependent manner with LC3-I to LC3-II conversion (Figure 3A). In addition, in AGS cells at 24 hr after *H. pylori* ATCC700392 (s1m1VacA) eradication, intracellular CagA levels were significantly decreased, as compared to 15 hr after eradication; conversion of LC3-I to LC3-II was clearly evident (Figure 3B). Conversely, in WT-A10 cells exposed to *H. pylori* F57 (VacA-negative), ot210 (s1m2VacA), or SS1 (s2m2VacA) culture supernatant, there was no decrease in intracellular CagA levels, and no LC3-I to LC3-II conversion was detected (Figure S1A). Moreover, in AGS cells at 24 hr after *H. pylori* F57 (VacA-negative), ot210 (s1m2VacA), or SS1 (s2m2VacA) eradication, there was no decrease in intracellular CagA, and no LC3-I to LC3-II conversion was detected (Figure S1B). To investigate the function of CagA from each strain, we examined the tyrosine phosphorylation level of each CagA protein. All the CagA proteins were phosphorylated (Figure S1C), suggesting that those CagA species behaved similarly in delivered host cells.

In CagA-expressing WT-A10 cells incubated with m1VacA for 24 hr, a significant m1VacA-dependent decrease in intracellular CagA levels was observed along with LC3-I to LC3-II conversion (Figure 3C). Autophagy inhibitors (5 mM 3MA or 50 nM Wort) repressed the LC3-I to LC3-II conversion induced by m1VacA and significantly increased intracellular CagA levels (Figure 3D). In CagA-expressing WT-A10 cells incubated with m2VacA, intracellular CagA was not degraded and LC3-I to LC3-II conversion was not observed (Figure S1D). In addition, at 24 hr after *H. pylori* F57 (VacA-negative) eradication, there was a significant increase in CagA, as compared with cells infected with *H. pylori* ATCC700392 (s1m1VacA) (Figure S1E). The increase of intracellular CagA produced by *H. pylori* F57 (VacA-negative) was reduced by the addition of 60 nM m1VacA, in contrast to the addition of 60 nM m2VacA (Figure S1E). To evaluate the biological activity of VacA, we examined the vacuolation activity of m1VacA and m2VacA. Both proteins induced vacuolation in CagA-expressing WT-A10 cells in a dose-dependent manner, although m1VacA induced stronger vacuolation activity than m2VacA (Figure S1F). Our observations demonstrate that the autophagy responsible for CagA degradation is induced by m1VacA in gastric epithelial cells, independent of vacuolating cytotoxicity.

We recently found that low-density lipoprotein receptor-related protein-1 (LRP1) was one of the VacA receptors that

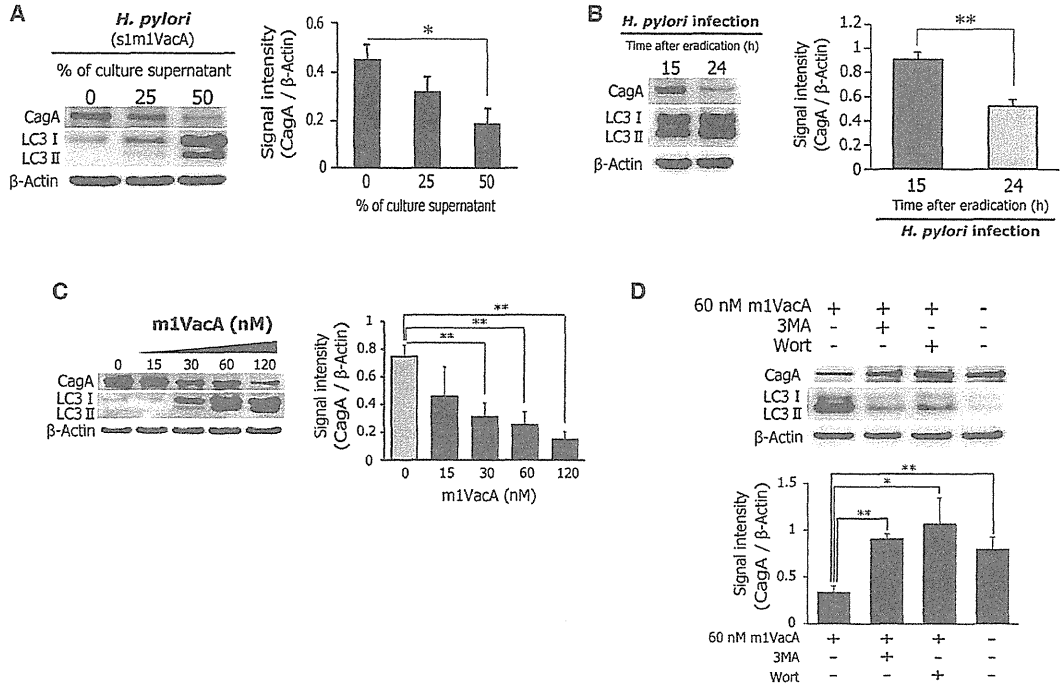

Figure 3. Autophagy, Causing CagA Degradation, Is Induced by m1VacA

(A) CagA-expressing WT-A10 cells were stimulated with *H. pylori* ATCC700392 (s1m1VacA) culture supernatant, and intracellular CagA and LC3-I to LC3-II conversion were examined. Data represent the mean ± SD of three independent assays; *$p < 0.05$.

(B) AGS cells infected with *H. pylori* (s1m1VacA) for 5 hr were incubated in a medium containing antibiotic for 15 and 24 hr, and intracellular CagA and LC3-I to LC3-II conversion were examined. Data represent the mean ± SD of three independent assays; **$p < 0.01$.

(C) CagA-expressing WT-A10 cells were incubated with m1VacA for 24 hr, and intracellular CagA and LC3-I to LC3-II conversion were examined. Data represent the mean ± SD of three independent assays; **$p < 0.01$.

(D) CagA-expressing WT-A10 cells, stimulated by m1VacA, were incubated with an autophagy inhibitor (5 mM 3MA or 50 nM Wort) for 24 hr, and intracellular CagA and LC3-I to LC3-II conversion were examined. Data represent the mean ± SD of three independent assays; *$p < 0.05$, **$p < 0.01$. See also Figure S1.

mediate induction of autophagy (Yahiro et al., 2012). Then, to examine the relevance of LRP1 for the induction of autophagy-mediated CagA degradation, we constructed specific LRP1-knockdown AGS cells using small interfering RNAs (siRNAs) (Figure S1G). The LRP1 knockdown repressed the LC3-I to LC3-II conversion, resulting in the inhibition of CagA degradation (Figure S1H). This result indicates that LRP1 is required for the induction of autophagy-mediated CagA degradation in response to m1VacA. Next, to compare the binding ability of m1VacA and m2VacA to LRP1, we performed an immunoprecipitation assay with anti-LRP1. An 87 kDa fragment of VacA was detected by western blotting with an anti-VacA antibody in the anti-LRP1 immunoprecipitates from AGS cells infected with *H. pylori* ATCC700392 (s1m1VacA) (Figure S1I). In contrast, VacA was not detected in the anti-LRP1 immunoprecipitates from AGS cells infected with *H. pylori* ot210 (s1m2VacA) (Figure S1I). This result demonstrates that m1VacA, but not m2VacA, has a binding potential to LRP1.

p53 Downregulation via Increased MDM2-Phosphorylation Induces Autophagy, Causing CagA Degradation

p53 inactivation by chemical inhibition or knockdown induces autophagy via the inhibition of mTOR. To investigate the induction of autophagy associated with CagA degradation, we examined p53 expression in AGS cells after *H. pylori* infection. In AGS cells at 15 and 24 hr after eradication of *H. pylori* ATCC700392 (s1m1VacA), p53 expression was significantly decreased and LC3-I to LC3-II conversion was clearly detected (Figure 4A). We then examined the mechanisms of p53 downregulation, focusing on posttranslational mechanisms, since *H. pylori*-infected AGS cells have been reported to show no change in *p53* mRNA expression (Wei et al., 2010). It is well known that p53 can be degraded by ubiquitination and proteasomal degradation pathways and that murine double minute 2 (MDM2) is the main E3 ubiquitin ligase that mediates p53 degradation. MDM2 expression was unaltered in AGS cells after *H. pylori* ATCC700392 (s1m1VacA) infection (Figure 4B). MDM2 is activated by phosphorylation at Ser166 (pMDM2) (Zhou et al., 2001). At 15 and 24 hr after the eradication of *H. pylori* ATCC700392 (s1m1VacA), pMDM2 levels were significantly increased (Figure 4B). Conversely, in AGS cells after *H. pylori* F57 (VacA-negative), ot210 (s1m2VacA), or SS1 (s2m2VacA) infection, neither a decrease in p53 expression nor an increase in pMDM2 was noted (Figure S2).

We then examined the relationship between p53 downregulation and intracellular CagA stability. The specific